S.O.S -
Development of a Scatterometer Ocean Stress Product

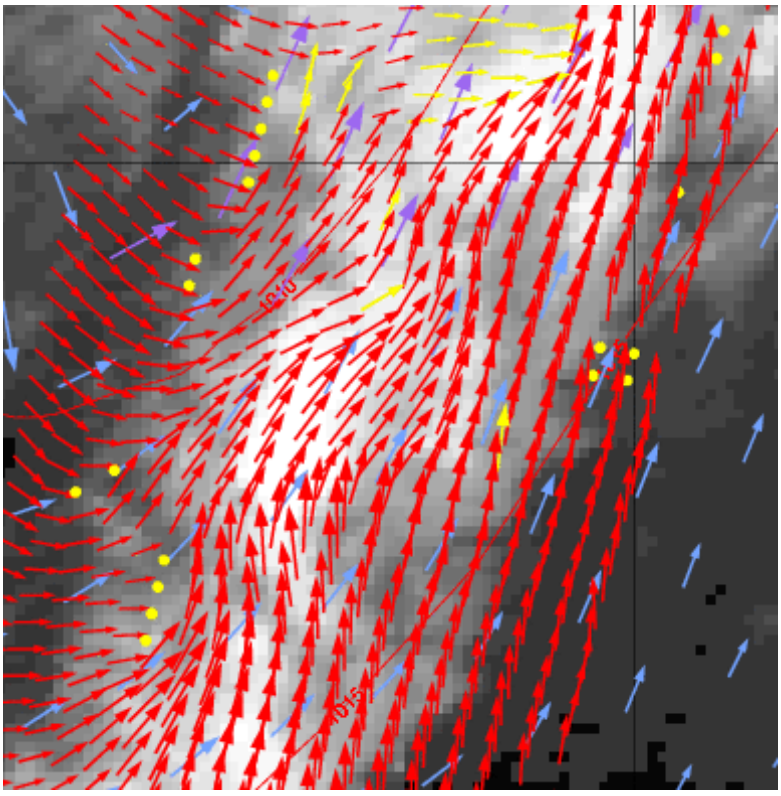

June 2007

Cover: ERS-2 scatterometer winds (red) on 28 August 2006 showing a train of Rossby waves in the North Atlantic. The blue arrows in the background depict background NWP model winds (KNMI HiRLAM) that generally do not resolve such weather phenomenon. The METEOSAT IR grey image in the background is consistent with the scatterometer surface winds.

Table of Contents

1 Preface

KNMI extended its contribution to the EUMETSAT Climate Monitoring Satellite Application Facility (CM-SAF, hosted by DWD) by developing a scatterometer ocean stress (SOS) gridded product. The SOS project is initiated by two sections of KNMI in two different departments, namely the Oceanographic Research division (OO) within the Department of Climate research and Seismology (KS), and the division on Observation Research (RW) in the Observations and Modelling department (WM).

Ten years of ESA ERS-1 and ERS-2 scatterometer swath data have been reprocessed with the most recent ERS Scatterometer Data Processor as developed within the OSI and NWP SAFs and processed to gridded SOS products. This activity fits into the ESA Data User Programme (DUP) acknowledging ESA for the provision of the ERS-1 and ERS-2 scatterometer data. Currently KNMI seeks support for the further development, extension (into the NASA/NOAA Seawinds and METOP-A ASCAT era starting in 1999) and maintenance of the SOS product. This report has been written by

Ad Stoffelen (Project leader; WM-RW),

Geert Jan van Oldenborgh (KS-OO),

Jos de Kloe (WM-RW),

Marcos Portabella (Un. Of Barcelona; visiting WM-RW),

Anton Verhoef (WM-RW)

2 Overview SOS project

2.1 Scope

The CM-SAF working group on ocean parameters solicited proposals to meet the core requirements on ocean parameters for climate applications in its Development Phase, DP. Wind stress forces motion in the ocean and in turn the motion in the ocean determines the weather and climate in large portions of the world. Scatterometer Ocean Stress, SOS, products incorporate wind stress, as measured by a scatterometer, to establish climatologies of this important parameter. Almost ten years of ERS scatterometer data are reprocessed using software developed within the Ocean and Sea Ice and Numerical Weather Prediction SAFs.

In a later stage, by reprocessing SeaWinds scatterometer data on QuikScat and ADEOS-II, and ASCAT on EPS, the time series of scatterometer ocean stress (SOS) may be extended. Moreover, resources permitting, the abundant wind measurements from passive sensors could be added to the database for improved time and space coverage.

2.2 Motivation

A 10-year SOS product of high quality may be useful for the understanding of several processes on climate time scales:

Wind forcing is essential in the El Niño Southern Oscillation (ENSO) phenomenon, but large uncertainties of about 30% exist in its structure and amplitude. This remains one of the main uncertainties in the modelling of ENSO. A homogeneous data set of high quality would much advance research on the prediction and mechanisms of ENSO seasonal forecasting. Vialard (2000) emphasizes that wind stress is certainly the most important forcing in the tropics. Moreover, ENSO plays a key role in the earth' climate.

There is now much evidence that the onset of ENSO depends on westerly wind events (bursts) that only last a few days, which is small compared to the time scale of ENSO. Complementary to the TAO buoy array, it would be useful to have continuous wind stress time series of high temporal and spatial resolution, extending beyond the TAO buoy area. This would aid in the understanding of the unexplained variability of these wind events from year to year.

Also in the tropical Atlantic Ocean there is a pattern of ocean-atmosphere interaction similar to ENSO, however, more moderate in amplitude and faster. Again, a high-quality SOS product would much improve the picture as compared to the current situation with the PIRATA buoys. The detailed observation of these phenomena is crucial for understanding climate variability issues.

Besides tropical needs, obvious applications of SOS would be among others in the modelling of the Antarctic circumpolar current, forcing of the southern oceans, research on the variability and occurrence of storms, and forcing in complex basins, e.g., the Mediterranean.

Within the NWP SAF and the OSI SAF scatterometer processing software and scatterometer products are developed at KNMI. This includes sophisticated calibration procedures for the measurements and for the resulting winds. A new geophysical retrieval algorithm had been established for ERS and ASCAT measurements. Moreover, KNMI has developed a technique to

investigate and validate geophysical retrievals by a triple collocation technique (Stoffelen, 1998). This technique is now frequently used in the scatterometer and altimeter community for wind calibration purposes. KNMI extended this technique to incorporate comparisons with the surface stress parameter with the aim to reduce the geophysical retrieval error. Other existing processing centres producing climate data sets do not use the geophysical model function recommended by the ESA/EUMETSAT ASCAT Science Advisory Group (Hersbach et al, 2006), nor do they use the same sophisticated validation tools. For climate research purposes, it is of interest to reprocess the ERS data in order to get an accurate and uniform 10-year time series, using the most up-to-date processing scheme, and to make these data easily available.

2.3 Background

Climate applications have strong requirements for reprocessing capability and availability of long time series of high quality products (e.g., Vialard, 2000). The KNMI climate explorer therefore contains sets of observations and model data over long time periods and of high quality. This also includes wind stress data, e.g., from ECMWF re-analysis (ERA15), and NCEP/NCAR re-analyses, FSU and CERSAT ERS analyses, and TAO buoy data. In this section some background information is provided on the characteristics of these data sources in comparison to the proposed SOS.

Wind stress can be computed from conventional platforms, such as ship or buoy. However, since these represent sparse and local measurements, only temporally and spatially course climatologies can be computed. Moreover, these systems measure the atmospheric flow at measurement height that can vary between 4 m and 60 m, and are thus not a direct measure of surface stress. Stress computation requires the transformation of these winds by Planetary Boundary Layer (PBL) parameterisation schemes in order to represent the sea surface conditions. These PBL schemes are not very accurate and contain transformation errors of typically 30%.

Atmospheric observations are combined into atmospheric analyses through NWP data assimilation systems. Re-analysis efforts are ongoing to produce long and consistent time series. Ideally, it would be best to incorporate scatterometer wind stress observations into such re-analysis projects. However, data assimilation of satellite products is not yet a completely mastered technique and direct estimates of wind stress from satellite instruments can provide a better product. This is particularly the case in the tropical region, but also in semi-enclosed seas such as the Mediterranean. Note that the abundant provision of surface wind stress data from scatterometers is not accompanied by a similarly abundant provision of upper air (wind) data. As such, it is extremely difficult in an NWP system to provide a spatially consistent analysis at the resolution of a scatterometer (25-50 km). Several studies have shown that the response of an ocean model depends on whether the wind stress forcing is by NWP analyses or by climatologies directly based on observation systems.

Such responses depend on data general quality, for example as expressed in table 1, but also on the spatial structures resolved by an observation system or NWP model. Table 1 illustrates that the general accuracy of data depends on geographical region; NWP models are known to be relatively poor in the tropical region. However, this region is very important for climate studies.

Vector RMS error [m/s]	TAO buoys - Tropical	NDBC – Extra-tropical

Buoy	1.6	2.8
Scatterometer	1.8	2.5
NWP model	2.2	1.6

Table 1. Vector error estimates by wind triple collocation method for a data set collocated with TAO tropical buoys, second column (preliminary result), and NDBC extra tropical buoys, last column (Stoffelen, 1998).

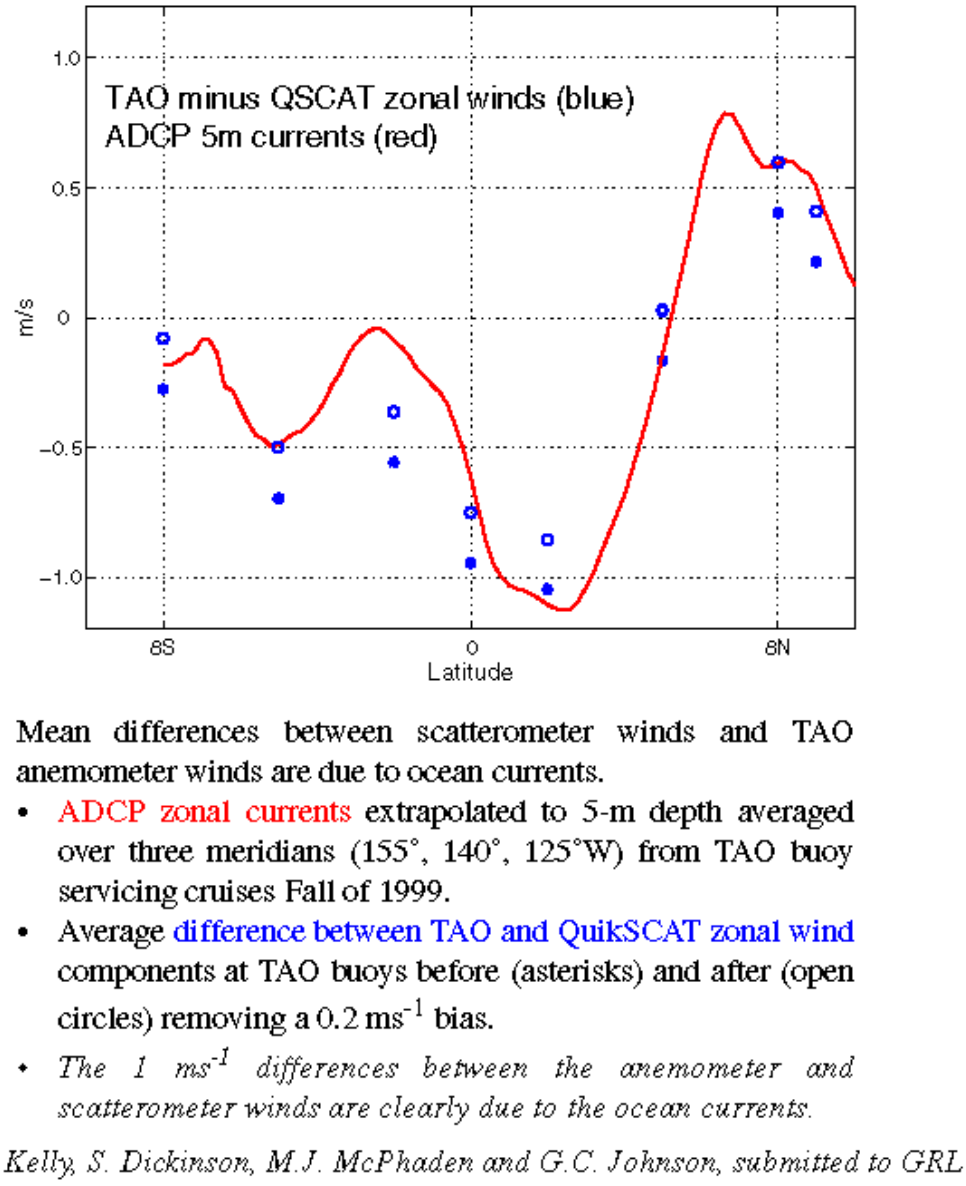

Figure 1a. (Courtesy: Kathryn Kelly, APL, Un. of Washington, Seattle, USA)

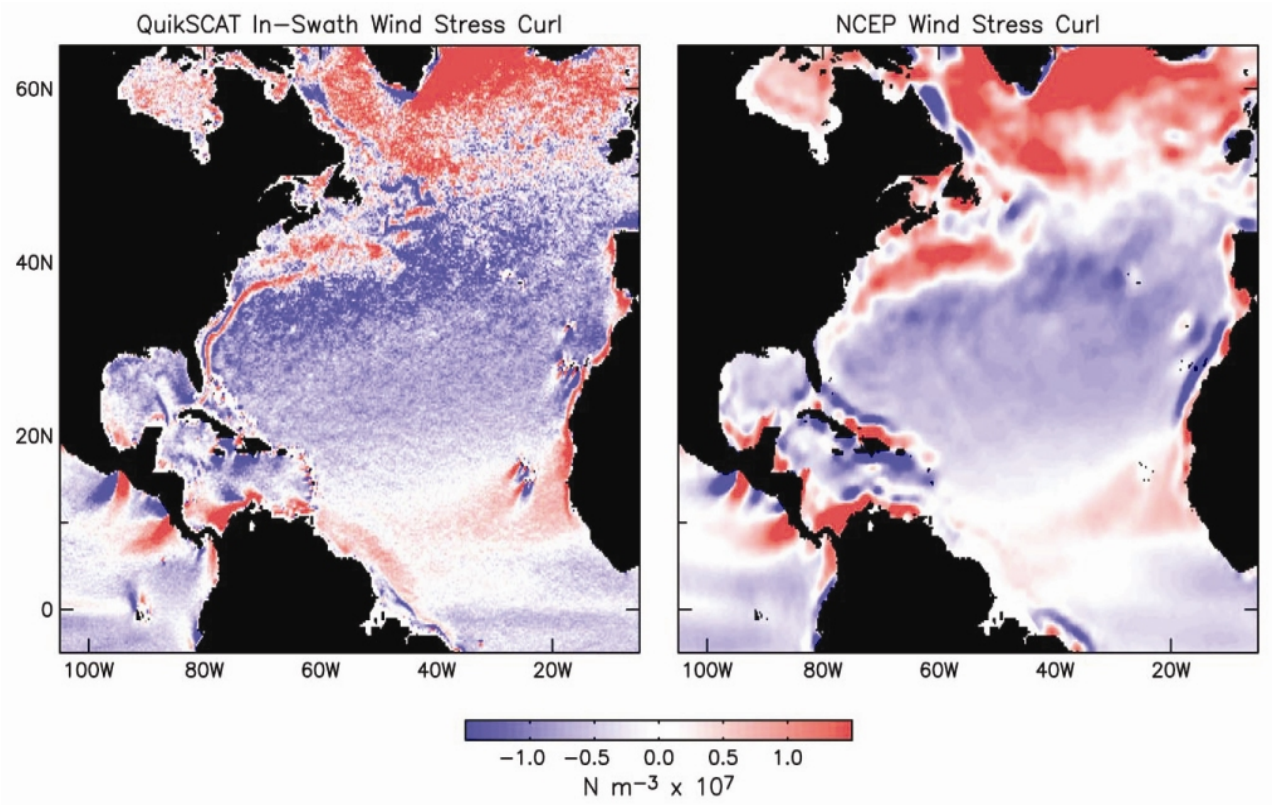

Figure 1b. 4-year Average Wind Stress Curl over the period from August '99 to July '03 as computed from SeaWinds scatterometer winds (left) and the NCEP operational NWP model (right). (© Chelton, Schlax, Freilich, Milliff, *Science*, 2004)

Buoy wind observations and, by implication, the NWP analyses that exploit these data use a fixed frame of reference. However, the wind stress depends on the difference of motion between atmosphere and ocean. Figure 1a shows an example of the effects of ocean currents and thus of the errors that may be introduced by computing ocean wind stress from buoy winds.

A scatterometer measures the electromagnetic radiation scattered back from ocean gravity-capillary waves and it is difficult to validate quantitatively the relationship between the roughness elements associated with gravity-capillary waves and the measurements. As such, empirical techniques are employed to relate microwave ocean backscatter with geophysical variables. Since the launch of the First Earth Remote Sensing Satellite, ERS-1 (on 17 July, 1991), with on board the active microwave instrument operating at 5.4 GHz (C band) numerous retrieval optimisations and validation studies have been carried out. Usually the retrieved products from satellite scatterometers are validated by collocation with NWP model (European Centre for Medium Range Forecast, (ECMWF)) background winds, and/or buoy measurements (Stoffelen, 1998). A multitude of wind observations is available at a reference height of 10 m, and as such scatterometer winds are traditionally related to 10m winds.

Using collocated meteorological observations during the RENE-91 experiment (from 16 September to 10 December, 1991) and NWP daily forecast winds, the ERS-1 scatterometer winds are calibrated and the CMOD4 algorithm (Stoffelen, 1998) is selected by ESA for wind retrieval from the ERS-2 scatterometer data (Offiler, 1994). In particular, wind direction retrieval is superior for CMOD4. More recently, CMOD5 has been derived, which provides a higher-order correction to CMOD4 wind speeds, in particular at hurricane-force wind speeds.

CMOD5 and the long series of comprehensive buoy measurements (see e.g. Chelton et al, 2001) provide a good basis to intercompare scatterometer and NWP model and buoy wind stress data in a triple collocation exercise (see Stoffelen, 1998).

The web application "KNMI Climate Explorer" offers the standard download capabilities and some visualisation possibilities. Its strength lies in the capabilities to quickly correlate and compare data with a lot of other data, such as other estimates of the wind stress (see above). The data retrieval and visualisation capabilities of the LDEO system, http://ingrid.ldeo.columbia.edu, are more advanced, but the data analysis and comparison capabilities are more restricted

Activities in the field of stress retrieval from scatterometers exist at JPL, COAPS, and SOC. The added value of the proposed KNMI wind stress product with respect to other scatterometer-based products that are available thus lies in

- Use of ESA/EUMETSAT ASCAT SAG recommended wind retrieval procedures resulting in best performances for wind speed and wind direction;
- Consistency between near-real-time wind products (OSI SAF) and climate stress products CM-SAF);
- Sophisticated methodology to minimise the geophysical retrieval error by a triple collocation comparison scheme using scatterometer observations, buoy measurements, and NWP model analyses for validation;
- Production of stress fields made available through a data analysis and comparison tool, the KNMI Climate Explorer.

2.4 Objectives

2.4.1 Proposal for CM-SAF development phase

Scatterometer wind products and processing are limited to level 2 in NWP and OSI SAF. In the oceanographic community, there is much need for higher level products that can be used directly to force ocean models. Such products are already available at KNMI through the “Climate Explorer”. Here, we propose to add the level 3 ERS scatterometer product in the “Climate Explorer” and put the data available to the world-wide research community.

What is of particular interest in a scatterometer is that it provides a measure of the relative motion between atmosphere and ocean, not the absolute motion of the atmosphere as a buoy does (e.g., see figure 1a). The forcing of the ocean obviously depends on relative motion. Furthermore, we propose to deliver surface stress as output, and not 10-m wind, to facilitate use in the oceanographic community. In order to achieve this, an existing triple collocation database of scatterometer, TAO buoy, and ECMWF boundary layer parameters will be exploited (e.g., see table 1).

The data is made available to researchers

- The web application "KNMI Climate Explorer" offers the standard download capabilities and some visualisation possibilities. Its strength lies in the capabilities to quickly correlate and compare data with a lot of other data.

2.4.2 Future plans

Figure 1b illustrates the ocean inertial features that may be obtained from scatterometer data. These structures are obviously relevant to force ocean eddies. Due to the low-pass filtering characteristics of NWP data assimilation systems, these observed structures are lost in NWP fields (figure 1b, left). As such the SOS product for SeaWinds and ASCAT may be crucial for realistic ocean forcing, both in operational oceanography and climate studies.

Our intention is to commit to routine / operational responsibilities. At a later stage we would add SeaWinds scatterometer data to the database. The SeaWinds data coverage is representative of ASCAT, whereas the ERS coverage is more limited. On the longer term, ASCAT reprocessing and higher level products could be envisaged. Moreover, resources permitting, the abundant winds from passive microwave sounders may be investigated for use in the CM-SAF wind stress package as these present some of the same advantages as scatterometers, though lack good information on wind direction.

2.5 Deliverables

The processing algorithms for ERS data are described, tested, and verified in the OSI SAF DP and IOP and will be used here. New stress algorithms are described scientifically, technically, are tested, verified, and validated in this report.

The SOS development in the CM-SAF DP aimed at the following deliverables

1. Wind stress vectors on an along-track/cross track grid at a resolution of 50 km in a simple format specifying latitude, longitude, meridional wind stress component, zonal stress component, and stress amplitude;
2. Fields of the wind stress vectors on a lat-lon-time grid with a spatial resolution of 50 km and temporal resolutions of one month and one day in the netcdf format with the COARDS conventions.
3. Fields of higher moments of the wind stress, on a lat-lon-time grid with a spatial resolution of 50 km and a temporal resolution of one month in the netcdf format with the COARDS conventions.
4. Web-based tools to let the user define products at other time scales which are then available for download and study in the same way as the standard monthly fields.

All produced data cover the period 1991-2000 and are freely available through a set of web pages that also allow visualisation and comparisons with other estimates of the wind stress.

2.6 Work packages

The above deliverables result from a set of work packages with associated tasks.

1) Co-ordination of the different work packages and of communication with and reporting to the CM-SAF steering group.
2) Acquisition and reprocessing of all ERS data using OSI SAF produce and control software:
   - Retrieve full ERS scatterometer data set from ESA or ECMWF;
   - Ocean calibration using ECMWF re-analysis data;
   - Reprocessing and monitoring (validation);
3) Conversion of scatterometer 10-m wind to scatterometer surface stress;
   - Literature review;

- Exploitation of triple collocation data bases with NWP model, buoy, and scatterometer data to tune and test the conversion algorithm;
- Conversion of ERS wind time series to stress time series;

4) Conversion from level 2 to level 3 product (monthly gridded data) and incorporation into the KNMI "Climate Explorer".
5) Extension of the Climate Explorer to include intelligent time-averaging routines to construct sensible fields from the sub sampled data that are available.
6) Investigation of wind-stress conversion using SeaWinds

- Literature review;
- Comparison of SOS data bases with SeaWinds scatterometer data to validate the conversion algorithm;

An overview of the activities is provided in the diagram below.

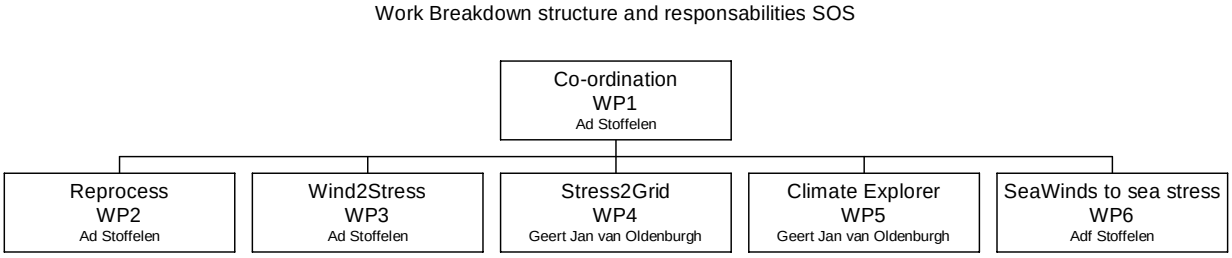

3 Wind to Stress conversion

3.1 Wind stress data sources

Wind stress can be computed from conventional platform observations, such as ship or buoy. These systems measure the atmospheric flow at a measurement height that can vary between 4 m and 60 m, and are thus not a direct measure of surface stress. Stress computation requires the transformation of these winds by Planetary Boundary Layer (PBL) parameterisation schemes in order to represent the sea surface conditions. These PBL schemes and more in particular, the Surface Layer (SL) schemes embedded in the PBL schemes, have improved accuracy over the years (*Smith et al., 1992*; *Donelan et al., 1993*; *Taylor and Yelland*, 2001; *Bourassa*, 2006) although they still contain transformation errors.

Furthermore, buoy wind observations and, by implication, the NWP analyses that exploit these data use a fixed frame of reference. However, the wind stress depends on the difference of motion between atmosphere and ocean. *Kelly et al.* (2001) show that the ocean currents do produce a significant bias in the buoy-derived wind stress estimations. In contrast, they show that scatterometer observations provide a measure of the relative motion between atmosphere and ocean, and therefore can potentially provide accurate wind stress information.

Since the conventional systems represent sparse and local measurements, only temporally and spatially course climatologies can be computed. Several studies have shown that the response of an ocean model depends on whether the wind stress forcing is by Numerical Weather Prediction (NWP) analyses or by climatologies directly based on observation systems. Such responses depend on data general quality but also on the spatial structures resolved by an observation system or NWP model. *Stoffelen* (1998a) illustrates that the general accuracy of data depends on geographical region and, in particular, NWP models are known to be relatively poor in the tropical region. However, as already mentioned, this region is very important for climate studies.

Several authors have pointed to the mesoscale wave number gap in NWP wind datasets (e.g., *Chelton et. al., 2004*; *Chelton and Schlax, 1996*; and *Stoffelen, 1996*). This gap is caused by the aforementioned sparse conventional observations at the sea surface, but also aloft since NWP data assimilation systems are 4-dimensional (4D) in nature and thus require 4D observations to achieve uniform quality. In fact, mesoscale atmospheric waves are poorly observed. Scatterometers, however, do have the capability to observe the surface component of such waves. Moreover, scatterometers provide information on the inertial scale of ocean models and thus can potentially provide essential information to drive ocean models (e.g., *Milliff, 2005*; *Chelton et al., 2004*; *Chelton and Schlax, 1996*).

3.1.1 How do we measure wind stress from scatterometers?

A scatterometer measures the electromagnetic radiation scattered back from ocean gravity-capillary waves and it is difficult to validate quantitatively the relationship between the roughness elements associated with gravity-capillary waves and the measurements. As such, empirical techniques are employed to relate microwave ocean backscatter with geophysical variables. Since the launch of the Earth Remote Sensing Satellites, ERS-1 (on 17 July, 1991) and ERS-2 (on 21 April, 1995), with on board the active microwave instrument (*Attema, 1991*) operating at 5.4 GHz (C band) numerous retrieval optimisations and validation studies have been carried out. Usually the retrieved products from satellite scatterometers are validated by collocation with

NWP model (e.g., European Centre for Medium Range Forecast, ECMWF) background winds, and/or buoy measurements (*Stoffelen, 1998a*). A multitude of wind observations is available at a reference height of 10 m, and as such scatterometer winds are traditionally related to 10m winds. For ERS scatterometers, the function that relates the 10-meter wind to the backscatter measurements, i.e., the Geophysical Model Function (GMF), and is used nowadays by ESA and KNMI for wind retrieval is the so-called CMOD-5 (*Hersbach et al., 2006*).

Stoffelen (1998a) shows that for varying ocean wind conditions, the backscatter measurements vary along a well-defined conical surface in the 3D measurement space, i.e., the measurements depend on two geophysical variables or a 2D vector. CMOD-5 indeed well explains the distribution of backscatter measurements in measurement space.

Chelton et al. (2001) and *Stoffelen* (2002) show a high correlation between scatterometer-retrieved winds and wind stress. In fact, scatterometers measure sea surface roughness (rather than 10-meter wind), which is highly correlated with the wind stress. So, if one collocated wind stress or its equivalent value at 10-meter height (i.e., 10-m neutral wind) to CMOD-5 winds and estimated their relationship, one would obtain a CMOD-5 stress model (or CMOD-5 neutral wind model) providing the same conical fits in 3D measurement space. For example, *Milliff and Morzel* (2001) use a 10-m neutral wind GMF to transform SeaWinds scatterometer winds to stress.

The problem is that wind stress observations, as computed from buoy or NWP models, are not perfect. As already mentioned, the SL schemes which convert buoy or NWP wind observations into wind stress observations, are inaccurate. Therefore, in order to define a scatterometer wind-speed[1]-to-stress transformation, we need to account for the uncertainties of all data sources.

3.1.2 Surface layer models

There are several SL models in the literature that could be used to compute wind stress from buoy observations and/or NWP output. Given the inaccuracy of such models, prior to transforming scatterometer winds to stress, we first take a close look at them and compare their performance. For such purpose, we pick two of the most commonly used models, i.e., the LKB model (*Liu et al., 1979*) and the ECMWF SL model (*Beljaars*, 1997), and compare them in chapter 3. Such intercomparison, however, does not provide an independent framework to assess the accuracy of the SL models.

3.1.3 Triple collocations

Stoffelen (1998b) shows that given a triple collocation dataset, e.g., scatterometer, buoy, and NWP observations, the uncertainty of the three observing systems can be uniquely determined, provided that one of the systems is used as reference for calibration (scaling) of the other two systems. As such, in chapter 4, we perform the triple collocation exercise as described by *Stoffelen* (1998b), using scatterometer winds as calibration reference, to assess the random accuracy and scaling properties of both buoy and NWP wind stress derived from the SL models.

[1] Note that the transformation only refers to wind and stress intensities since the direction of the air flow is assumed to be constant in the SL.

The triple collocation exercise is also used to investigate whether the ERS scatterometer-derived (CMOD-5) winds are closer to a 10-m neutral wind (uniquely related to the wind stress) rather than to 10-m real wind, given the uncertainties of the different data sources and SL models used in the triple collocation. A scatterometer wind-to-stress transformation is finally recommended in order to produce an SOS product from ERS scatterometer winds. Finally, a summary of the work and recommendations for future developments of the SOS product are presented in chapter 5.

As a first step towards a global ERS SOS product, and given the crucial role of wind stress in the tropics, we put here our focus in this work. This implies a focus on atmospheric stability and humidity effects as well. On the other hand, effects due to wave age or fetch are known to be relevant in the extra-tropics and therefore not considered here but in a companion report (*Portabella and Stoffelen, 2006*).

3.2 Dataset

A triple collocation dataset for the year 2000 is generated to carry out the work described in this report. The three observing systems used in this dataset are the ERS-2 scatterometer, the TAO/PIRATA buoy array, and the ECMWF model.

KNMI produces the scatterometer wind and stress products of the EUMETSAT-sponsored OSI and Climate Monitoring (CM) SAFs, and develops the wind software in the Numerical Weather Prediction (NWP) SAF. In the framework of these SAFs, KNMI has developed an ERS scatterometer data processing (ESDP) package for the generation of operational wind products. As such, ERS-2 ESDP 10-m winds are used in this study.

The National Oceanic Atmospheric Administration (NOAA) TAO and PIRATA buoy arrays are located in the tropical Pacific and Atlantic oceans, respectively (see Figure 2). 10-minute average winds (at 4 meter height) together with other surface layer relevant parameters, such as sea surface temperature (SST), air temperature (T) and relative humidity (rh), are retrieved from the following NOAA sites: http://www.pmel.noaa.gov/tao and http://www.pmel.noaa.gov/pirata). ECMWF ERA-40 lowest level (approximately 10 meter height) winds, T, specific humidity (q), pressure (p), SST, surface pressure (sp) and Charnock parameters are retrieved from the ECMWF MARS archive.

The triple collocations are performed in the following way. The ESDP collocation software is used to spatially and temporally interpolate the ECMWF ERA-40 forecast data to the ERS-2 scatterometer data acquisition location and time, respectively. Then the ECMWF-ERS dataset is collocated to the TAO/PIRATA buoy dataset using the following criteria: only observations separated less than 25 km in distance and 30 minutes in time are included in the ECMWF-ERS-TAO/PIRATA triple collocation dataset. In practice, most of the collocations are within 12.5 km and 10 minutes, thus considerably reducing the collocation error, i.e., uncertainty due to spatial and temporal separation between collocated observations.

Several Quality Control (QC) procedures have been applied to this dataset. The nominal ESDP QC procedure is applied to the ERS-2 retrieved wind dataset and only the TAO/PIRATA data with the “highest quality” flag are used. Moreover, a 4-sigma test is performed to the triple collocated dataset as in *Stoffelen* (1998b).

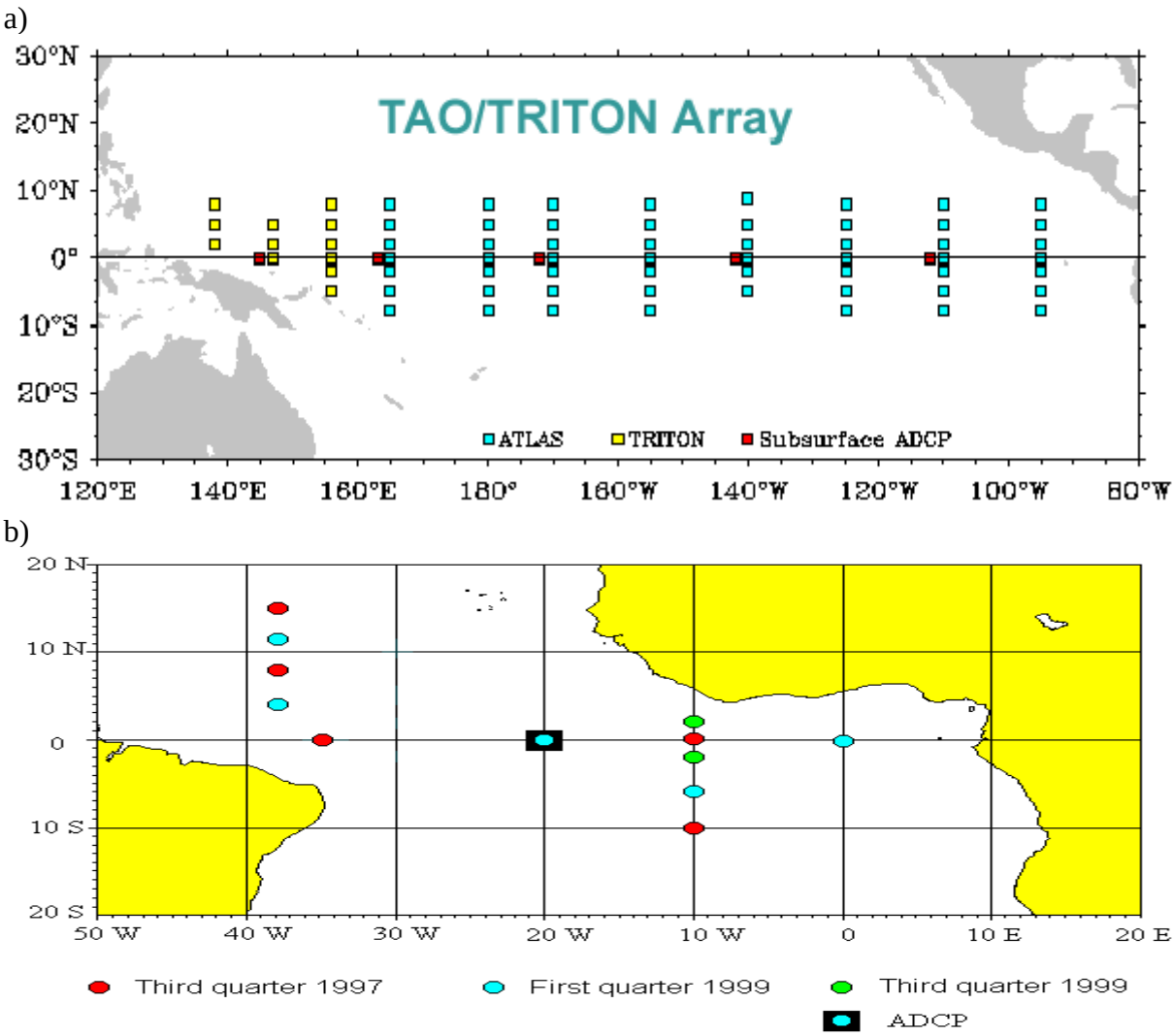

Figure 2. Geographical location of the NOAA TAO (top) and PIRATA (bottom) buoy arrays. Please note that no collocations were found for TRITON buoys (west of 160°E).

3.3 SL models

Most of the equations that describe the physical balances and the turbulent budgets in the lowest 10% of the PBL, i.e., the surface layer, cannot readily be solved, due either to the presence of highly nonlinear terms or the requirement for enormous in-situ data bases (*Geernaert, 1999*). One can alternatively characterize the flow's dominant dynamic, geometric, and temporal scales, which involve characteristic time, space, or velocity scales, by dimensionless groups of variables. The similarity theory, first postulated by *Monin and Obukov* (1954), states that there exists such groups of variables which have functional relationships to the flow field and/or fluxes, and these in turn can be used to characterize the behavior of the higher order terms of the above mentioned equations.

The surface layer is assumed to be a constant flux layer and it extends up to a few tens of meters above the surface. In the bulk parameterization of the similarity theory, the fluxes are determined with the transfer coefficients which relate the fluxes to the variables measured, i.e.,

$$H = c \cdot \rho \cdot C_H (U - U_s) \cdot (T_s - T),$$

$$E = \rho \cdot C_E (U - U_s) \cdot (q_s - q), \quad (1)$$

$$\tau = \rho \cdot C_D (U - U_s)^2,$$

where ρ and c are the density and isobaric specific heat of air; τ, H and E are the stress, heat and moisture fluxes; U, T and q are the wind speed, potential temperature and specific humidity at a reference height in the surface layer; U_s, T_s and q_s are the wind speed, temperature and specific humidity at the surface; and C_D, C_E and C_H are the transfer coefficients for momentum, heat and moisture, respectively. The C_D, also known as the drag coefficient, has been extensively studied. For deep water with large fetch, it has been expressed as a function of wind speed or assumed to be constant over a range of moderate wind speeds, e.g., *Businger*, (1975), *Garrat*, (1977). The transfer coefficients C_E and C_H are less well known and are usually treated as constants, and their variations with wind speed and stability neglected, e.g., *Pond et al.* (1974), and *Friehe and Schmitt* (1976).

The bulk transfer coefficients can be determined by integrating the U, T and q profiles. Close to the surface, the distributions of U, T and q are governed by diabatic processes. As such, the wind profile can be written as (e.g., *Businger 1973*):

$$u_* = \frac{k}{[\ln(\frac{z}{z_0}) - \psi(z/L)]} (U - U_s) \quad (2)$$

where k is the von Karman constant, $u_*^2 = \tau / \rho$ is the friction velocity, z is the height above the surface, z_0 is the roughness length for momentum, ψ is the stability function for momentum (positive, negative, and null, for unstable, stable, and neutral conditions, respectively) and L is the Monin-Obukhov length, which includes the effects of temperature and moisture fluctuations on buoyancy. Similar profiles to the one in Eq. 2 are also derived for the scale temperature (T_*) and the scale humidity (q_*) (see *Liu et al., 1979*). Since stability (z/L) depends on T and q, the set of 3 dimensionless profiles (u_*, T_*, and q_*) have to be solved at the same time.

In order to solve for u_*, the wind at certain height, among other parameters, is required (see section 3.3.1) and z_0 and L must be estimated (see Eq. 2). Once u_* is estimated, the SL models can be used to compute the wind at any height (within the SL) and any stability, e.g. neutral wind, just by modifying z and L, respectively, in Eq. 2. In other words, given a wind observation at certain height (within the SL), we can estimate the winds at any other height and stability, provided that we first go down to the surface and compute stress.

The discussion of air-sea transfer is not about the validity of the approach described above but generally about the details of parameter and function choices. As such, most SL models are based on Eqs. 1 and 2, and differences among them lie in the parameterization of L and/or z_0. This is the case for the two SL models used in this work, i.e., the LKB and the ECMWF SL models. Their similarities and differences are further discussed in the following section.

3.3.1 LKB versus ECMWF: formulation

The LKB and ECMWF SL models present the same roughness length function (see *Liu* et al., 1979, and *Beljaars*, 1997), which is written as:

$$z_0 = \frac{0.11 \cdot \nu}{u_*} + \frac{\alpha \cdot u_*^2}{g} \qquad (3)$$

where ν is the kinematic viscosity of the air (1.5×10^{-5} m^2/s), g is the gravitational constant of the Earth (9.8 m/s^2), and α is the Charnock parameter (see *Charnock, 1955*). However, the Charnock value, which is a sea-state parameter, is substantially different, i.e., 0.011 for LKB and around 0.018 for ECMWF SL (the latter is not a fixed value).

The same happens with the formulation of the stability function $\psi(z/L)$, which is identical for both models, although the computation of the *L* parameter (Monin-Obukhov length) differs from one another (see *Liu* et al., 1979, and *Beljaars*, 1997).

The stand-alone ECMWF SL model uses as input U, T, q, pressure (p), observation height (z), SST, surface pressure (sp), and Charnock data. Similar input is used in LKB; the main difference is that no Charnock input but a default value of 0.011 is used instead. If q information is not available, LKB also allows relative humidity (rh) observations as input. Both SL models can solve for wind stress provided that U, T, and SST are available. That is, when humidity and pressure observations are not available, default values are used instead. Those values are slightly different, i.e., relative humidity (rh) of 0.8 and sp=1013 hPa for LKB versus rh=1 and sp=1000 hPa for ECMWF.

Another relevant aspect of these models is the convergence procedure the models use to solve for u_* (and T_* and q_*). That is, u_* depends on two unknowns, z_0 and ψ (see Eq. 2), which in principle are independent from one another. In other words, the roughness length, which directly depends on the forcing (u_*) and the sea state (Charnock) as expressed in Eq. 3, should not be correlated with atmospheric stability (z/L). However, since the wind information available is always at certain height (z) above the surface, we need stability correction to go down to the surface and, as such, certain correlation between z_0 and z/L is inevitable. This is especially the case for LKB algorithm, which solves Eqs. 2 and 3 at the same time. In the case of ECMWF, the mentioned correlation is much smaller since z_0 (Eq. 3) is solved prior to z/L, making a set of assumptions about u_* and stability.

3.4 LKB and ECMWF comparison

In this section, we present some results of comparing the LKB model against the ECMWF SL model, using the TAO/PIRATA buoy data and the ECMWF data described in section 3.2.

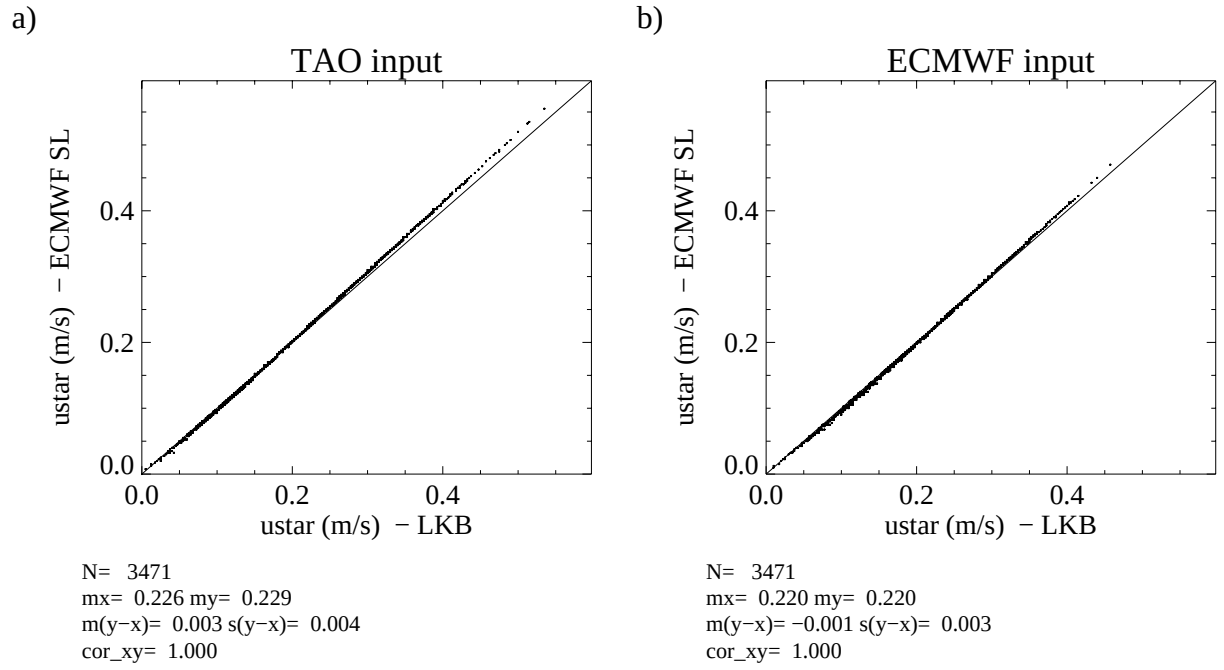

Figure 3. Two-dimensional histogram of LKB estimated u_* versus ECMWF SL estimated u_* for two different input datasets: TAO/PIRATA buoys (a) and ECMWF model output (b). N is the number of data; mx and my are the mean values along the x and y axis, respectively; m(y-x) and s(y-x) are the bias and the standard deviation with respect to the diagonal, respectively; and cor_xy is the correlation value between the x- and y-axis distributions.

Figure 3 shows the two-dimensional histogram of LKB estimated u_* versus ECMWF SL estimated u_* for two different input datasets: TAO/PIRATA buoys (left plot) and ECMWF model output (right plot). Since the two datasets contain different parameters (see discussion in section 3.2) and the two SL models allow somewhat different input (see section 3.3.1), we select the coincident parameters for all 4 combinations: U, T, and SST. As it is clearly discernible, the distribution lies on the diagonal, it is very narrow, and the correlation is 1, meaning that the estimated u_* is very similar, regardless of the SL model or the dataset used. In other words, the two models show very similar results. Moreover, very similar histograms to the ones in Figure 3 are produced when including q (from ECMWF dataset) or rh[1] (from TAO/PIRATA dataset) as input.

A 5% bias at high u_* values, especially visible in Figure 3a, needs to be explained, though. We know from earlier discussion that SL model differences must lie in the roughness length and the stability parameters. Therefore, we now take a closer look at them.

[1] ECMWF SL software can be adapted to allow rh as input.

3.4.1 Roughness term

Figure 4 shows the same as Figure 3, but for the z_0 parameter. Again, the correlation between the two models is striking. However, we clearly see the differences between the two model formulations. As discussed in section 3.3.1, the Charnock parameter is substantially different for both models, i.e., 0.011 for LKB and 0.018 (default value) for ECMWF. Therefore, for very low u_* values, where the viscosity term (first right-hand side term of Eq. 3) is dominant, the distribution lies on the diagonal (same z_0 for both models), and for higher u_*, where the Charnock term is dominant (second right-hand side term of Eq. 3), the distribution is off diagonal, with a slope which is given by the ratio between the Charnock values of both models.

Looking at Figures 4 and 3, one can easily realize that in order to achieve such good agreement in u_* (Figure 3), the stability term in Eq. 3 has to compensate for the difference in the roughness term between the two models. Given the fact that the roughness term is logarithmic, the difference between LKB roughness term and ECMWF roughness term is just a constant, i.e., $\ln\left(\frac{z}{z_0^{ECMWF}}\right) = \ln\left(\frac{z}{z_0^{LKB}}\right) - k$, where $k = \ln(\frac{\alpha^{ECMWF}}{\alpha^{LKB}}) \cong 0.5$. Since the roughness term $\ln\left(\frac{z}{z_0^{LKB}}\right)$ values vary between 13 (low z_0) and 9.5 (high z_0), provided that the stability term is relatively small in both models, there should be a bias of about 5% between ECMWF and LKB u_*, which is not present at low and mid u_* values (see Figure 3).

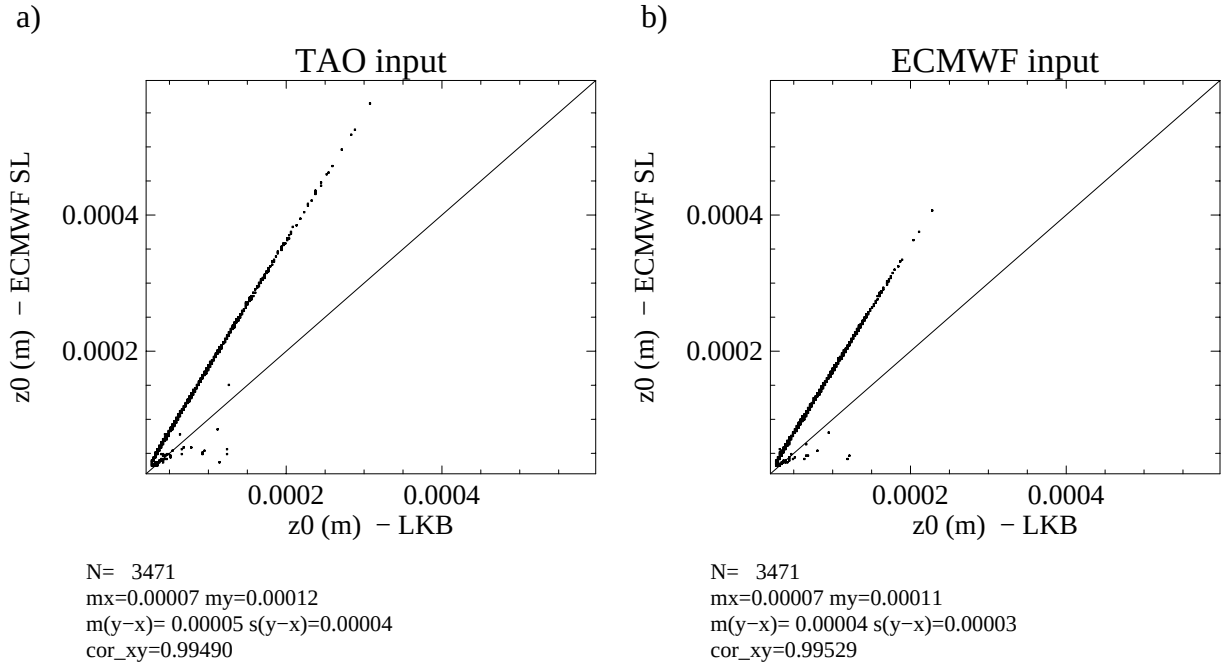

Figure 4. Same as Figure 3 but for the estimated z_0 parameter.

3.4.2 Stability term

Figure 5 shows the ratio between the roughness term and the stability term as a function of z_0 for both the LKB model (left plot) and the ECMWF SL model (right plot). As already discussed in section 3.3.1, the correlation between z_0 and stability (z/L) is larger for LKB than for ECMWF SL model. This is actually shown in these plots (note that the left plot shows higher correlation than the right plot). An interesting result here is that both plots show that the stability term is marginal (high ratio values) for high z_0 values. This is consistent with the bias observed in Figure 3, i.e., the constant *k* becomes relevant at increasing z_0, since the stability impact becomes marginal and $\ln\left(\frac{z}{z_0^{LKB}}\right)$ decreases. At low and medium z_0 values, we note from Figure 5 that LKB stability term is more relevant than the ECMWF stability term (i.e., there are larger accumulations at low ratio values in the left plot than in the right one). Since most of the observations in the tropics correspond to unstable situations ($\psi > 0$), the more relevant stability term for LKB compensates the larger z_0 values from ECMWF SL model, such that the resulting u_* values are very similar for both models.

Given the fact that both SL models use the same stability functions (ψ), we can easily prove that LKB estimates larger instability (higher negative z/L values) than ECMWF for low and medium z_0 values, i.e., low and medium u_* values. Figure 6 shows the histogram of the stability parameter (z/L) for both the LKB model (solid line) and the ECMWF SL model (dotted line). We note larger accumulations away from the origin (z/L = 0) for LKB than for ECMWF SL, indicating larger estimated instability in the former model.

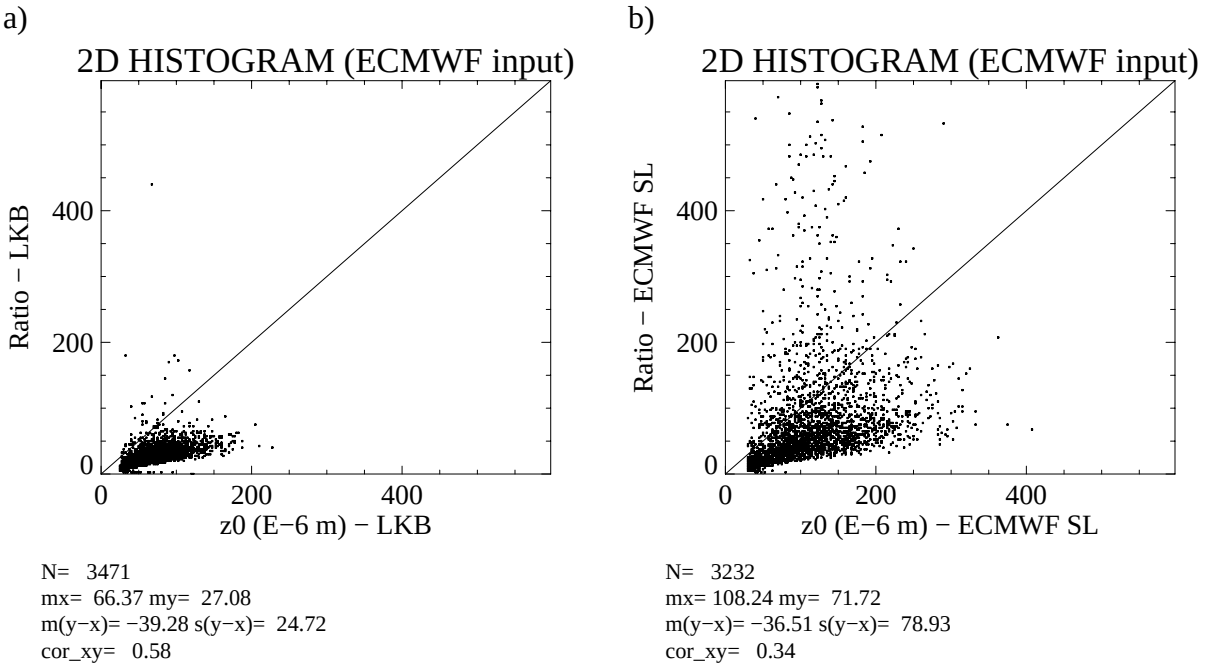

Figure 5. Ratio between the roughness term and the stability term as a function of z_0 for both the LKB model (a) and the ECMWF SL model (b). The legend is the same as for Figure 3.

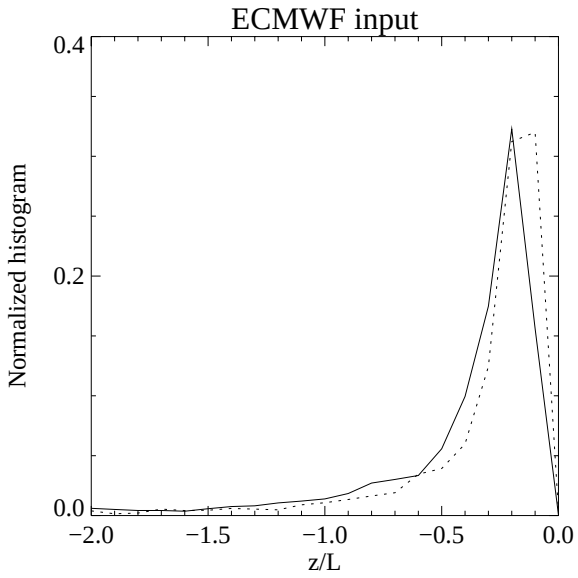

Figure 6. Normalized histogram of the stability parameter (z/L) for both the LKB model (solid) and the ECMWF SL model (dotted).

3.4.3 Charnock parameter

As mentioned in section 3.3.1, the Charnock parameter is fixed for LKB but not for ECMWF SL model. Up to now, results have been produced with fixed Charnock values (default values) for both models, i.e. 0.011 for LKB and 0.018 for ECMWF. Figure 7 shows a scatter plot of z_0 against u_*, as estimated by the ECMWF SL model, for TAO/PIRATA (left plot) and ECMWF (right plot) input datasets. For the former dataset, no Charnock is provided and therefore the default value is used; for the latter dataset, variable Charnock (i.e., sea-state dependent) values are used. Note that the right plot (variable Charnock) shows more scatter than the left plot (fixed Charnock). However, the scatter is modest. This is confirmed when reproducing Figure 3a with variable ECMWF Charnock input. The 2-D histogram (not shown) shoes only marginally larger spread (Standard Deviation or SD of 0.004) as compared to the one in Figure 3a (SD of 0.003). The main reason for this is that sea state in the tropics is rather smooth. This may not be the case in the extra-tropics, where the differences in the z_0 parameterization of both SL models (see section 3.3.1) can lead to more significant differences in the wind stress estimation. Further investigation is therefore required.

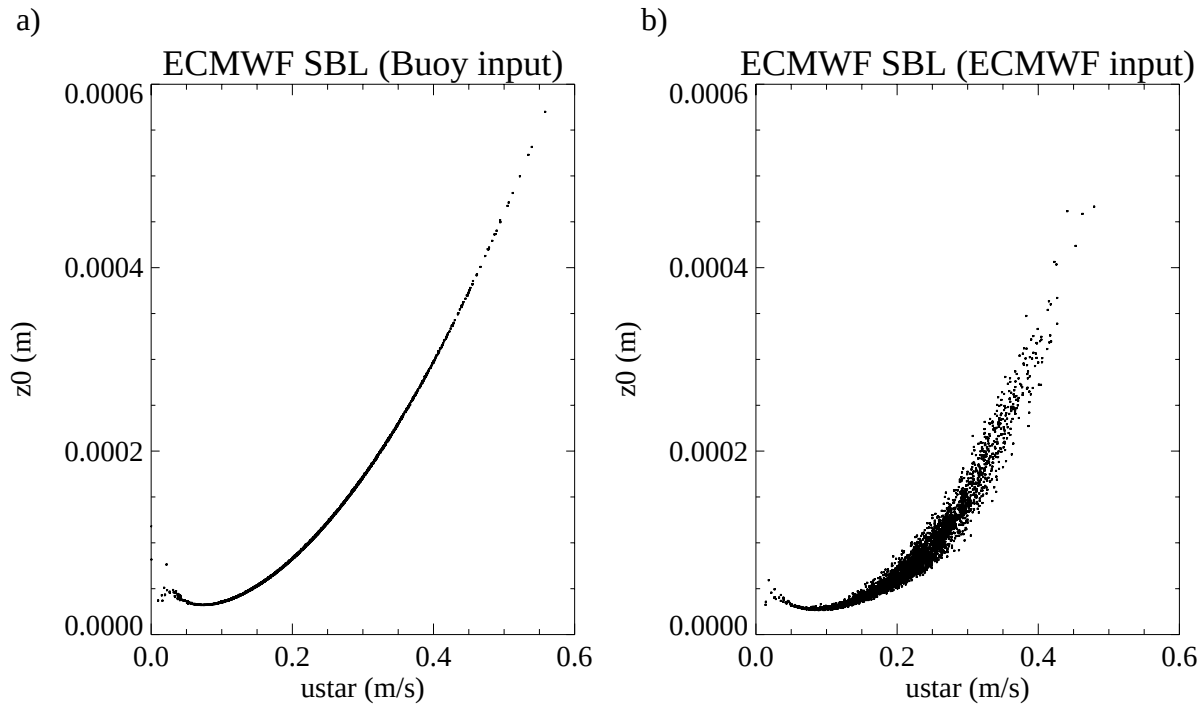

Figure 7. Scatter plot of ECMWF SL estimated z_0 against ECMWF SL estimated u_*, for TAO/PIRATA (a) and ECMWF (b) input datasets. The latter contains variable Charnock values.

3.4.4 TAO/PIRATA versus ECMWF observations

Another interesting feature in Figure 3 is that both SL models generate larger u_* values from buoy input (Figure 3a) than from ECMWF input (Figure 3b). Figures 8a shows the distribution of u_* given by the LKB model, using buoy (solid) and ECMWF (dotted) input. The distributions are very similar for low u_* but different for medium and high u_* values, where the buoy input u_* are clearly larger than the ECMWF input. Similar distributions are shown in Figure 8b for the ECMWF SL model. This is mainly due to the wind observations, as shown in Figure 8c. The latter shows the same distributions as for Figures 8a and 8b but for observed wind speed. The buoy and the ECMWF wind speed distributions are very similar for medium and high winds. However, since buoy data are closer to the surface ($z = 4$ m) than ECMWF lowest level observations ($z \cong 10$ m), the corresponding u_* values are larger for buoy input data than for ECMWF input data (see logarithmic wind profile of Eq. 2). In other words, TAO/PIRATA wind speed observations are relatively high as compared to ECMWF winds.

We also note that differences between the u_* distributions at high u_* values in Figure 8b are somewhat larger than in Figure 8a. This is due to the already mentioned z_0 parameterization differences between the SL models, which causes some bias at high u_*, as shown in Figure 3.

3.4.5 Neutral winds

The impact of stability on wind stress estimations is often measured by the difference between the actual wind (U) and its equivalent neutral wind (U_n), i.e., the wind that results from estimating u_*, given a wind observation at certain height z and under certain atmospheric stability (z/L), and using such u_* to solve Eq. 2 at the same height z assuming neutral stability (i.e., ψ=0).

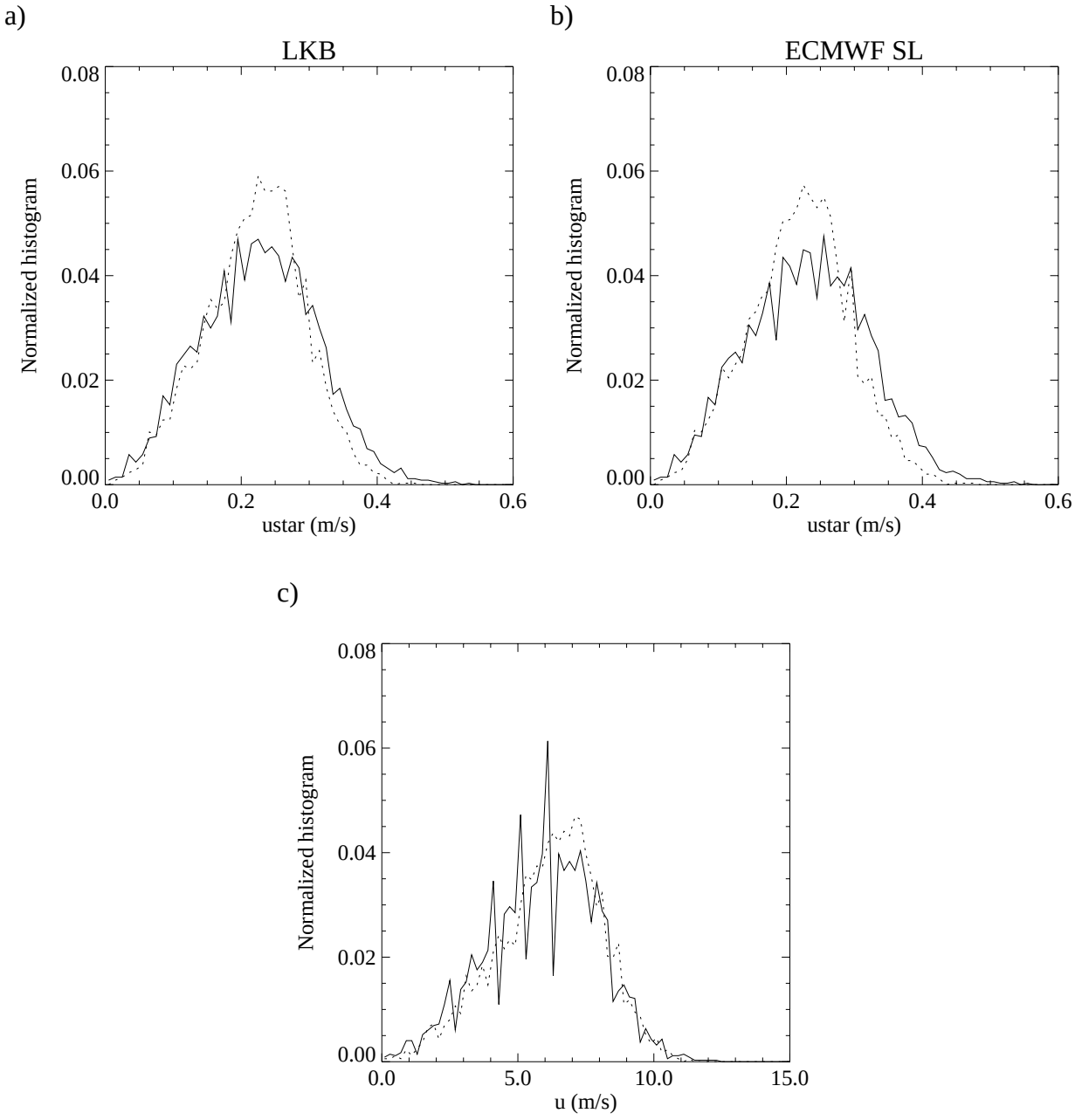

Figure 8. Histograms of ECMWF SL estimated u_* (a), LKB estimated u_* (b), and observed wind speeds (c), for TAO/PIRATA (solid) and ECMWF (dotted) data.

Figure 9 shows the difference between U_n and U as a function of U using the LKB model, for TAO/PIRATA (left plot) and ECMWF (right plot) input datasets. It is clear that the difference is larger for ECMWF input as compared to buoy input. This is mainly due to the logarithmic nature of the wind profiles with height and the fact that ECMWF observations are higher above the surface than TAO/PIRATA data (see discussion of Figure 8).

Figure 9 also shows that stability effects are small, in the order of the surface current effects (within ±0.5 m/s and a SD of ~0.1 m/s). Differences between neutral winds and actual wind tend to increase for low winds (below 3 m/s) and then slightly decrease for increasing speeds. The same pattern is produced when using ECMWF SL model instead of LKB (not shown). This is in contradiction with Liu and Tang (1996), who showed a 10% difference between neutral and actual winds, for winds between 4 m/s and 10 m/s, using the LKB model and TAO input data. Further discussion on this matter can be found in Appendix A.

In conclusion, LKB and ECMWF SL models produce very similar u_* values, except for high winds, where a 5% bias of the latter with respect to the former is found. The differences in the roughness parameterization are somewhat compensated by differences in the stability parameterization, except for high winds, where the stability term is negligible as compared to the roughness term. Differences between the (non sea state dependent) LKB and the (sea state dependent) ECMWF SL are expected to be larger in the extra-tropics, where sea state is substantially rougher than in the tropics.

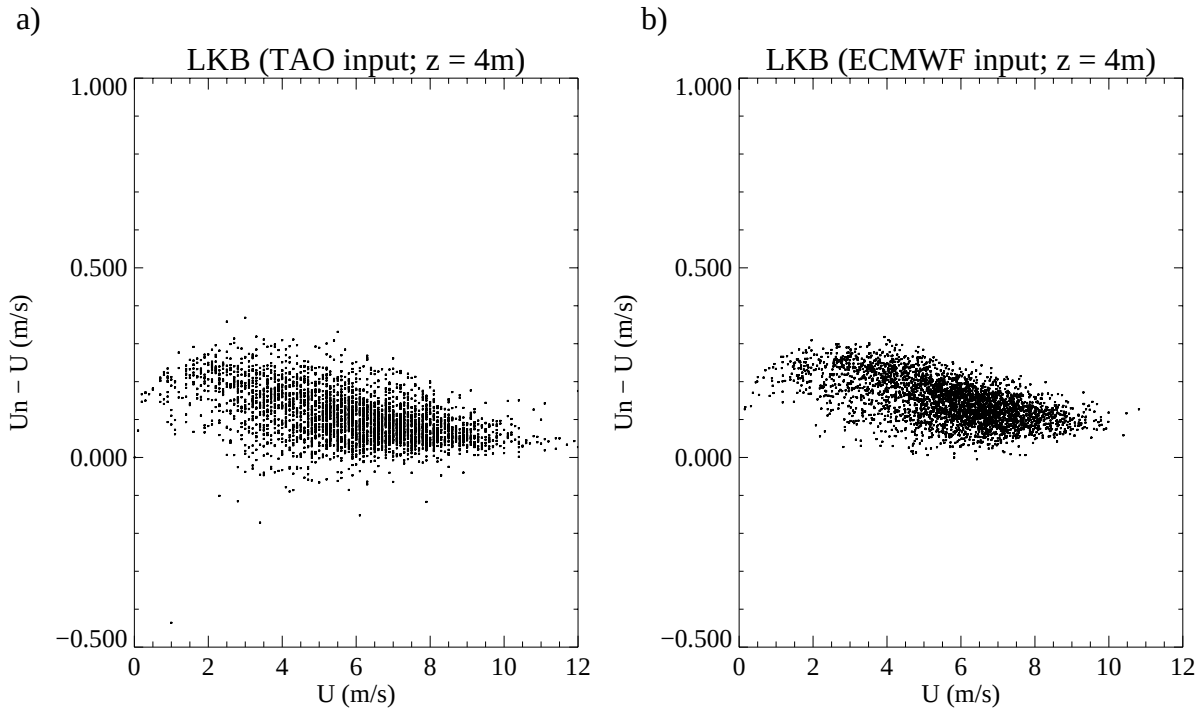

Figure 9. Difference between the LKB estimated U_n and U as a function of U, for TAO/PIRATA (a) and ECMWF (b) input datasets, at 4 m height.

3.5 Error assessment using LKB and ECMWF SL models

In remote sensing, validation or calibration activities can only be done properly when the full error characteristics of the data are known. In practice, the problem is that prior knowledge on the full error characteristics is seldom available. *Stoffelen* (1998b) shows that simultaneous error modeling and calibration can be achieved by using triple collocations.

When the three observing systems represent the same spatial scales, the triple collocation procedure can resolve the uncertainty of the three systems, provided that one of them is used as reference for calibration. When the systems do not represent the same resolution, we have to take into account the spatial representativeness error[1]. In particular, we need to make an assumption on the correlation of the spatial representativeness error, i.e., the (true) variance common to the two systems that can resolve the smaller scales[2].

In our case, we have one system, i.e., ECMWF that can only resolve large scales (> 200 km) and two systems, i.e., buoy and scatterometer that can resolve smaller scales. Since the scatterometer resolves wind scales of about 50 km, the true variance on spatial scales of 50 to 200 km is resolved by both scatterometer and buoys, but not by ECMWF. For three similar observing systems to the ones used in this work, i.e., NOAA buoy winds, ERS scatterometer winds, and National Centers for Environmental Prediction (NCEP) model winds, *Stoffelen* (1998b) estimated a correlated representativeness error (r^2) of 0.75 m^2/s^2 in the extra-tropics. In our case, and because of the generally lower small-scale wind variability in the tropics (trade winds) with respect to the extra-tropics, we assume an r^2 of 0.25 m^2/s^2 for the 50-to-200 km scale true variance.

3.5.1 Triple collocation error assessment

As mentioned in section 1, we can use the triple collocation exercise to assess the performance of the two SL models that we have compared in section 3.3, i.e., LKB and ECMWF. That is, we use the SL models to convert TAO/PIRATA and ECMWF wind observations to any reference height (e.g., 4 m, 10 m) and then estimate the errors of such buoy and NWP converted wind "observations", using ERS scatterometer CMOD-5 winds as reference system for calibration.

Table 2 shows the true variability and the observation error for each dataset, when LKB is used to produce the (buoy and NWP) wind datasets at 10-m height. Note that the scores are given in terms of wind component SD rather than wind component variance (square of SD value) since the former is most commonly used to refer to wind variability and observation errors. The true variability is substantially smaller (3.12 m/s and 4.89 m/s SD for u and v components, respectively) than the extra-tropical values estimated by Stoffelen (1998b) (4.68 m/s and 5.24 m/s SD for u and v components, respectively).

[1] When comparing two observation systems with different resolution, the variability of the higher resolution system at the scales that are not resolved by the lower resolution system may be interpreted as error, i.e., the spatial representativeness error. In fact, this variability is resolved true variance of the higher resolution system.
[2] This common variance is, in fact, the resolved true variance embedded in the representativeness error of both systems.

The correlated part of the representativeness error, as mentioned above, represents the common variance in the higher resolution systems, i.e., the scatterometer and the buoys. Therefore, when performing data interpretation for high resolution applications, e.g., development of 25-km or 50-km wind products, this common variance is considered as part of the true variance as well as part of the error (lack of high-resolution information) of the lower resolution system, i.e., NWP model. Table 2 accounts for such interpretation. However, when looking at lower resolution applications, e.g., NWP data assimilation, this common variance cannot be resolved and is therefore interpreted as part of the (spatial representativeness) error of the higher resolution systems, i.e., scatterometer and buoy. Table 3 shows the same as Table 2 but accounting for the latter interpretation. We note that differences between the two tables are not large since the assumed r^2 value is small compared to true and error variance values.

When ECMWF SL model is used (instead of LKB) to produce the (buoy and NWP) wind datasets at 10-m height, the triple collocation results (not shown) are almost identical to the ones in Tables 3 and 2. That is, the performance of both SL models is comparable.

Table 2 Estimates of the wind component SD of the true distribution and the errors of the scatterometer, LKB-derived 10 m buoy and ECMWF winds, for 50-km scale wind.

	True wind	Scatterometer	Buoy	ECMWF
u component (m/s)	3.16	0.93	1.08	1.57
v component (m/s)	4.91	0.71	1.01	1.30

Table 3 Same as Table 2, but for NWP-scale applications (~200 km).

	True wind	Scatterometer	Buoy	ECMWF
u component (m/s)	3.12	1.05	1.19	1.49
v component (m/s)	4.88	0.87	1.12	1.20

The same exercise is repeated using buoy and NWP winds at 4 m height. The results (not shown) are very similar in terms of true variability and errors of the different sources, also denoting the similar performance of both SL models. These results are in line with the results of section 3.3, where both models were showing little differences.

However, when performing triple collocation, the scaling factor for buoy (i.e., the buoy-to-scatterometer wind calibration value) is much closer to one at a reference height of 4 m than at 10 m, meaning that scatterometer winds should be interpreted as 4-m winds rather than 10-m winds.

Table 4 Estimates of the wind component SD of the true distribution and the errors of the scatterometer, LKB-derived 10 m buoy and ECMWF neutral winds, for 50-km scale wind

	True wind	Scatterometer	Buoy	ECMWF
u component (m/s)	3.15	0.94	1.08	1.57
v component (m/s)	4.91	0.70	1.01	1.31

Table 5 Same as Table 4, but for NWP-scale applications (~200 km).

	True wind	Scatterometer	Buoy	ECMWF
u component (m/s)	3.11	1.06	1.19	1.49
v component (m/s)	4.88	0.87	1.13	1.21

3.6 Scatterometer wind interpretation

As discussed in the introduction, scatterometers are essentially observing wind stress. Therefore, one may expect scatterometer-derived winds to be best interpreted as equivalent neutral winds (i.e., stress) rather than real winds. In this section, we investigate the interpretation of scatterometer data by performing the triple collocation exercise for two different datasets:

a) ERS CMOD-5 winds, TAO/PIRATA real winds, and ECMWF real winds;

b) ERS CMOD-5 winds, TAO/PIRATA neutral winds, and ECMWF neutral winds.

The first dataset is the same as the one used in section 3.5.1. The second dataset is the same as the first one but for buoy and NWP converted neutral winds using either LKB or ECMWF SL model.

The true variability and error scores of dataset a) (see Tables 2 and 3) are almost identical to the scores obtained with dataset b) (see Tables 4 and 5), when using LKB model and 10 m height conversion and when using an exact fixed set of data points. The same conclusions are drawn when using ECMWF SL model and/or 4 m height conversion. This illustrates that scatterometer winds can explain the same true variability regardless of whether these are tested against real or neutral winds. The only significant difference between the two datasets results is in the scaling factor value[1], meaning that provided that we use the appropriate scaling in the scatterometer

[1] Since most of the times the Tropics present unstable stratification, the real winds are biased low with respect to the equivalent neutral winds at any reference height within the SL.

GMF (e.g., CMOD-5), scatterometer winds are as close to real winds than they are to equivalent neutral winds (or stress).

In order to reinforce such conclusion, and given the fact that CMOD-5 GMF was tuned to 10-m real (NWP) winds, we develop a "neutral" GMF by tuning our CMOD-5 real winds to neutral winds. Figure 11 shows the bias of CMOD-5 winds with respect to 10-m buoy real winds (solid) and 10-m buoy neutral winds (dotted) as a function of wind speed. By subtracting these two curves, i.e., about 0.2 m/s, we can derive a real-to-neutral scaling (dashed) that can be used to convert CMOD-5 real winds into neutral winds.

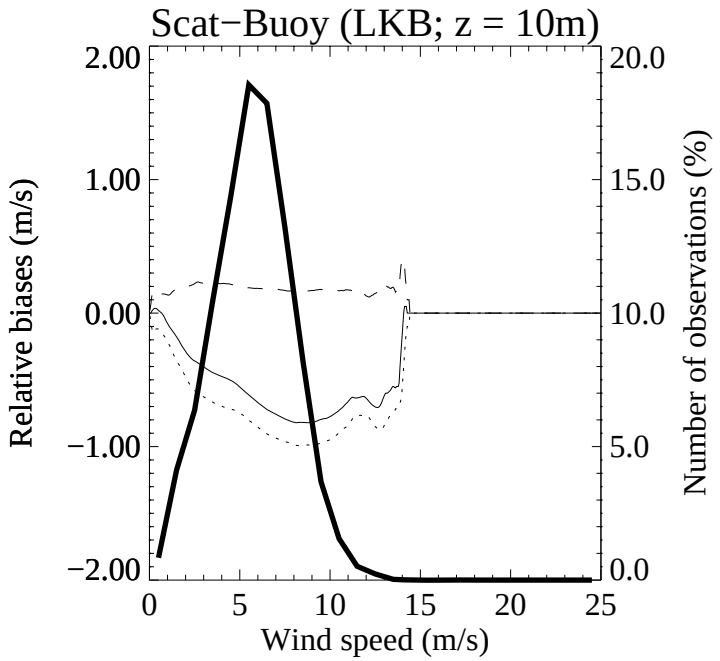

Figure 10. Relative bias of CMOD-5 winds with respect to 10-m buoy real winds (solid) and 10-m buoy neutral winds (dotted) as a function of wind speed. The buoy height conversion is performed with LKB model. The dashed curve corresponds to the solid minus the dotted curve.

We then perform the same triple collocation exercise as before but using the ERS converted neutral winds instead of CMOD-5 winds in datasets a) and b). As expected, the results are again very similar (not shown).

The fact that scatterometer winds are as close to real winds as to neutral winds can be explained as follows: on the one hand, the stability effects are small (see Fig. 8 in section 3.4), i.e., differences between real and neutral winds are subtle; on the other hand, SL models and the different observations (wind, SST, air temperature) used by the models to compute height conversions and neutral winds contain (spatial representativeness) errors, which in turn mask the already subtle differences between real and neutral winds.

3.7 Scatterometer wind-to-stress transformation

In order to obtain stress, first a well-calibrated scatterometer 10-m neutral wind is required. Then a SL model like LKB or ECMWF SL can be used to convert 10-m neutral winds to wind stress. In fact, since the most recently developed SL models (*Taylor and Yelland, 2001*; *Bourassa, 2006*) have similar performance up to 16 m/s (*Bourassa, 2006*), either one of them can be used to do the neutral-to-stress conversion. Since no stability information is needed to do this conversion, an independent scatterometer stress (SOS) product can be developed straightforwardly.

To obtain calibrated scatterometer 10-m neutral winds, a scatterometer-to-buoy correction (calibration) and a real-to-neutral wind conversion need to be applied on CMOD-5 winds as depicted in figure 12. The combined correction and conversion is represented by the dotted curve in Figure 10, which has a mean (absolute) value of 0.8 m/s. This differs somewhat from the combined correction value of 0.55 m/s found by *Hersbach et al.* (2006) and *Portabella and Stoffelen* (2006) doing the same triple collocation exercise but with extra-tropical datasets.

Several effects may lead to these differences between tropical and extra-tropical datasets. The most relevant are, on the one hand, the large wind variability in the extra-tropics, and, on the other hand, the effect of currents in the tropics. In order to recommend a final combined correction value, an analysis of the uncertainties of the triple collocation exercise (mainly produced by the mentioned effects) is performed. One way to analyze such uncertainties is to take the calibrated dataset (after triple collocation) and examine the residual biases buoy by buoy, i.e., scatterometer wind bias versus buoy and/or versus ECMWF at a particular buoy location. Table 6 shows the average and SD of the residual biases per buoy, for tropical buoys with more than 50 collocations. The uncertainty found (SD of about 0.2 m/s) is consistent with the expected effect of currents. However, a comparable result to that of Table 6 is found by *Portabella and Stoffelen* (2006) with an extra-tropical dataset, indicating that the uncertainty produced by the large wind variability in the extra-tropics, amongst other effects, is comparable to the buoy-to-buoy uncertainty in the tropics. In other words, both combined correction values (i.e., 0.8 m/s in the tropics and 0.55 m/s in the extra-tropics) have a similar degree of confidence and also both fall within the buoy-to-buoy spread as found in table 6 and the extratropics.

Therefore, we recommend adding 0.7 m/s (compromise between the tropical and the extra-tropical values) to CMOD-5 winds to obtain the scatterometer 10-m neutral winds.

Table 6 Average and SD of all local wind component residual biases (after wind calibration; per buoy location), for buoy and ECMWF winds against scatterometer winds.

	Buoy-Scat. U comp.	Buoy-Scat. V comp.	ECMWF-Scat. U comp.	ECMWF-Scat. V comp.
BIAS (m/s)	0.09	-0.02	0.21	-0.02
SD (m/s)	0.27	0.13	0.27	0.22

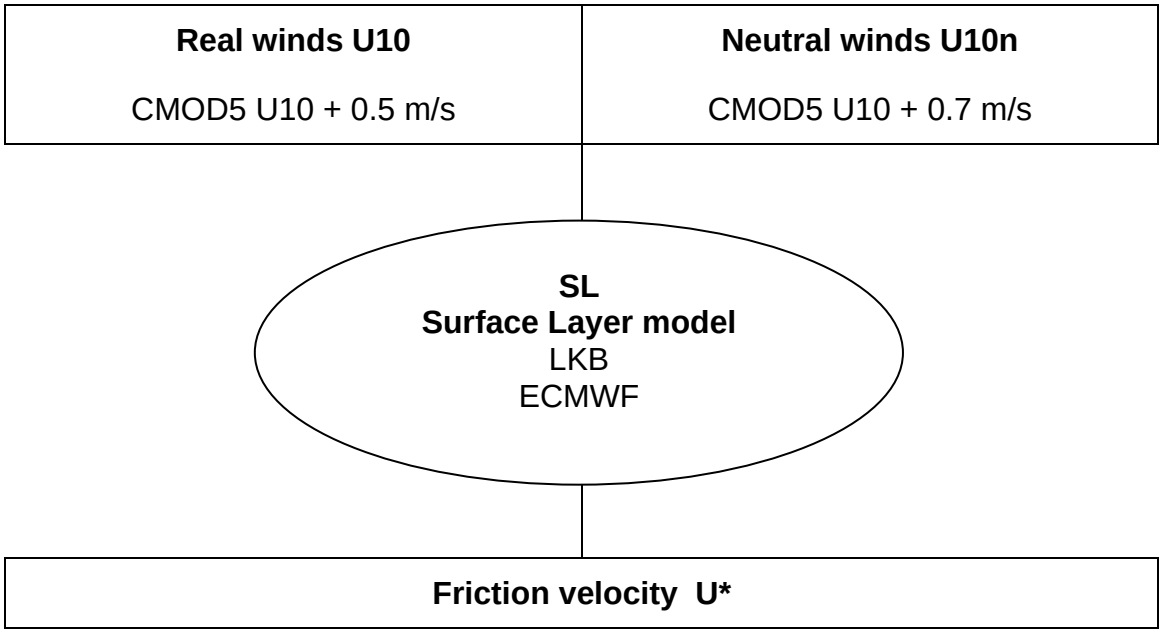

Figure 11. Schematic of recommended scatterometer wind and stress conversion. The well-validated CMOD5 winds at 10m height are used as basis for geophysical conversion to friction velocity. Either real or neutral 10m winds may be transformed to friction velocity by either LKB, ECMWF or any similar SL model.

3.8 Summary and recommendations wind and stress

We note the following conclusions and recommendation

3.8.1 Summary

In this work, we look for the most appropriate scatterometer wind-to-stress transformation, in order to produce a SOS product. For such purpose, a one-year (2000) triple collocated tropical dataset is used, i.e., ERS-2 scatterometer winds, TAO/PIRATA buoy data, and ECMWF model output. As a consequence, all comparisons are based on a fixed set of data points and uncertainties due to a difference in the number or location (e.g., by screening) of the inputs are absent. This is, the geophysical conditions for the comparisons are set fixed and a careful geophysical analysis follows.

First, a comparison between two commonly used SL models, i.e., LKB and ECMWF, is performed. The main difference between the two models is in the roughness length (z_0) and the stability (L) parameterizations. On the one hand, whereas LKB uses a constant Charnock value, ECMWF uses a substantially larger Charnock value. Since the ECMWF roughness parameterization is sea state dependent, its Charnock parameter is moreover somewhat variable.

On the other hand, LKB has larger instability (larger negative z/L values) with respect to ECMWF. This difference actually compensates for the difference in the roughness formulation for low and medium winds, such that the resulting stress values are very similar for both models. At high winds though, the stability term is much smaller than the roughness term and therefore the different roughness formulation results in some small stress bias between the two models.

Another relevant result of this comparison is that the bias due to the difference in the default Charnock values of both models remains the same when variable Charnock input is used for ECMWF SL model, and the SD of the difference between LKB and ECMWF estimated stress increases marginally.

A triple collocation exercise based on *Stoffelen* (1998b) is then conducted to assess the performance of the LKB and the ECMWF SL models. For such purpose, we use the SL models to estimate wind at different reference heights from the buoy and NWP datasets. For every SL model, we therefore generate two new buoy and NWP stress datasets (at each height), which are combined with the scatterometer winds (using the latter as reference for calibration) to estimate their individual errors. The results show that the uncertainty in the buoy wind dataset is smaller than in the NWP wind dataset. They also show a similar performance of both SL models. This is not surprising since most of the recently developed SL models (e.g., *Taylor and Yelland, 2001*; *Bourassa, 2006*) produce a similar stress for surface winds below 16 m/s (*Bourassa, 2006*).

The same triple collocation exercise is repeated but equivalent neutral buoy and NWP winds are used instead of real winds. True variability and error scores are almost identical to the ones of the previous exercise, and only scaling factors differ, meaning that scatterometer winds are as close to real winds than to neutral winds, provided that we use the appropriate conversion. A conversion is then derived, and to neutral converted winds are used instead of CMOD-5 winds in the triple collocation exercise. The results confirm the duality in the interpretation of scatterometer winds. An explanation for this duality is that the small stability effects (see section 3.4) are masked by the uncertainty in SL models and their inputs.

3.8.2 Recommendations

Finally, it is concluded that an independent ERS scatterometer stress (SOS) product can be obtained by adding 0.7 m/s to the CMOD-5 winds and use such result as the 10-m neutral wind input to a SL model, which is needed to compute stress, see figure 11. [Note that KNMI uses LKB SL model since it is widely used and publicly available.]

In general, differences in SL-derived wind stress magnitude are small for winds below 10 m/s, and it is only well above 10 m/s that the different roughness formulations produce large differences in the estimated stress (see also *Taylor et al., 2001*). Moreover, differences will occur in cases of extreme wind variability or air-sea temperature difference when wind-stress discrepancies may occur. Therefore, an extended extra-tropical dataset including high winds is being used at KNMI to further investigate the performance of the SL models at such wind regime, where the differences between models are expected to be more significant.

In the extra-tropics, differences between a non sea-state dependent SL model like LKB and a sea-state dependent model like ECMWF may be larger. In this respect, a similar validation to the work presented here in the extra-tropical regions is being carried out at KNMI (*Portabella and Stoffelen*, 2006). Moreover, additional SL models (e.g., *Taylor and Yelland, 2001*) may be considered for such dataset comparison including high winds.

The correlated spatial representativeness error of 0.25 m^2/s^2 assumed in here (see section 3.4) is a subjective extrapolation to the tropics of the extra-tropical value of 0.75 m^2/s^2 estimated by *Stoffelen* (1998b). The r^2 value does not significantly impact the wind-to-stress calibration results presented in section 3.6. However, it does somewhat affect the error assessment from section 3.5.1. That is, when comparing scatterometer or buoy data with ECMWF data, the r^2 is interpreted as part of the scatterometer/buoy error. As such, for larger r^2 values, although the uncorrelated scatterometer/buoy error remains the same, the "apparent" (as interpreted at NWP scales) scatterometer/buoy error, i.e., the sum of the uncorrelated error and r^2, increases and, consequently, the ECMWF error becomes smaller (see discussion on r^2 in section 3.5.1). Therefore, in order to make a more precise error assessment of the three observation systems used in this work, an accurate estimation of the correlated representativess error is required. *Stoffelen* (1996) presents a method to estimate r^2 for ERS scatterometer winds and buoy winds in the extra-tropics. *Vogelzang* (2006) extends this method to SeaWinds. Such method can be applied in the tropics as well.

4 Reprocessing of ERS swath wind data

4.1 Introduction

This chapter describes the reprocessing of ERS scatterometer data spanning the period of Sep 2, 1991 to Jan 17, 2001 and for both ERS 1 and ERS 2 missions. The output products are scatterometer wind data in BUFR and wind stress data in ASCII format. Lecomte et al (1999) describe the ERS scatterometer instrument products and their processing. More information on the ERS SCAT Data Processor (ESDP) and the wind product can be found in the ERS Scatterometer Product User Manual for the EUMETSAT Advanced Retransmission Service (EARS), published on the KNMI and EUMETSAT web sites.

4.1.1 Step 1: collocation of ERS data from MARS with model winds

The first step was performed at ECGATE, the gateway computing facility of ECMWF. ERS BUFR and ECMWF 40-year Reanalysis project, ERA40, GRIB model data were taken from MARS, the ECMWF Meteorological Archival and Retrieval System. The NWP model data provide forecast winds, and land-sea mask (LSM) and sea surface temperature (SST) at analysis time. Model data with analysis times of 00 and 12 GMT were used, with the forecast time steps +3, +6, +9, +12 and +15 hours. The NWP data were put into an appendix of the ERS BUFR messages for later use.

The model wind speed and direction at the satellite WVC (Wind Vector Cell) positions and acquisition times were obtained by interpolating the gridded NWP wind vector data with respect to position linearly and then time quadratically. For each WVC, the land fraction was calculated by averaging the land fractions of all NWP grid points within 80 kilometres of the WVC. Each grid point was weighted by $1/\text{distance}^2$. If this weighted land fraction was above 0.02, the WVC was flagged as ‘land’ and no winds were calculated in order to avoid land contamination. The SST of the WVC is again linearly interpolated from the four closest surrounding grid point SSTs of the model data. If the SST at the WVC position was below 273.16 K, the WVC was flagged as ‘sea ice’ and no winds were calculated in order to avoid sea ice contamination.

The output of the collocation process was sent to KNMI and stored in the KNMI MOS (Massa Opslag Systeem).

4.1.2 Step 2: wind processing on collocated ERS data

The data which have been collocated in step 1 were taken from the MOS, inverted winds were calculated and the resulting BUFR files were put back into the MOS. The 10-year reprocessing was done on a Linux workstation.

During the reprocessing, monitoring files were produced to assure the quality of the outputs for each 6 hours time interval (0:00-5:59, 6:00-11:59, 12:00-17:59 and 18:00-23:59 of each day). From these data, time series of Max. Likelihood Estimator (inversion residual or cone distance; *Stoffelen*, 1998a), Wind Speed Bias and Wind Component RMS were plotted for each quarter. The figures below show an example of the fourth quarter of 1992, showing a quite stable behaviour over this period.

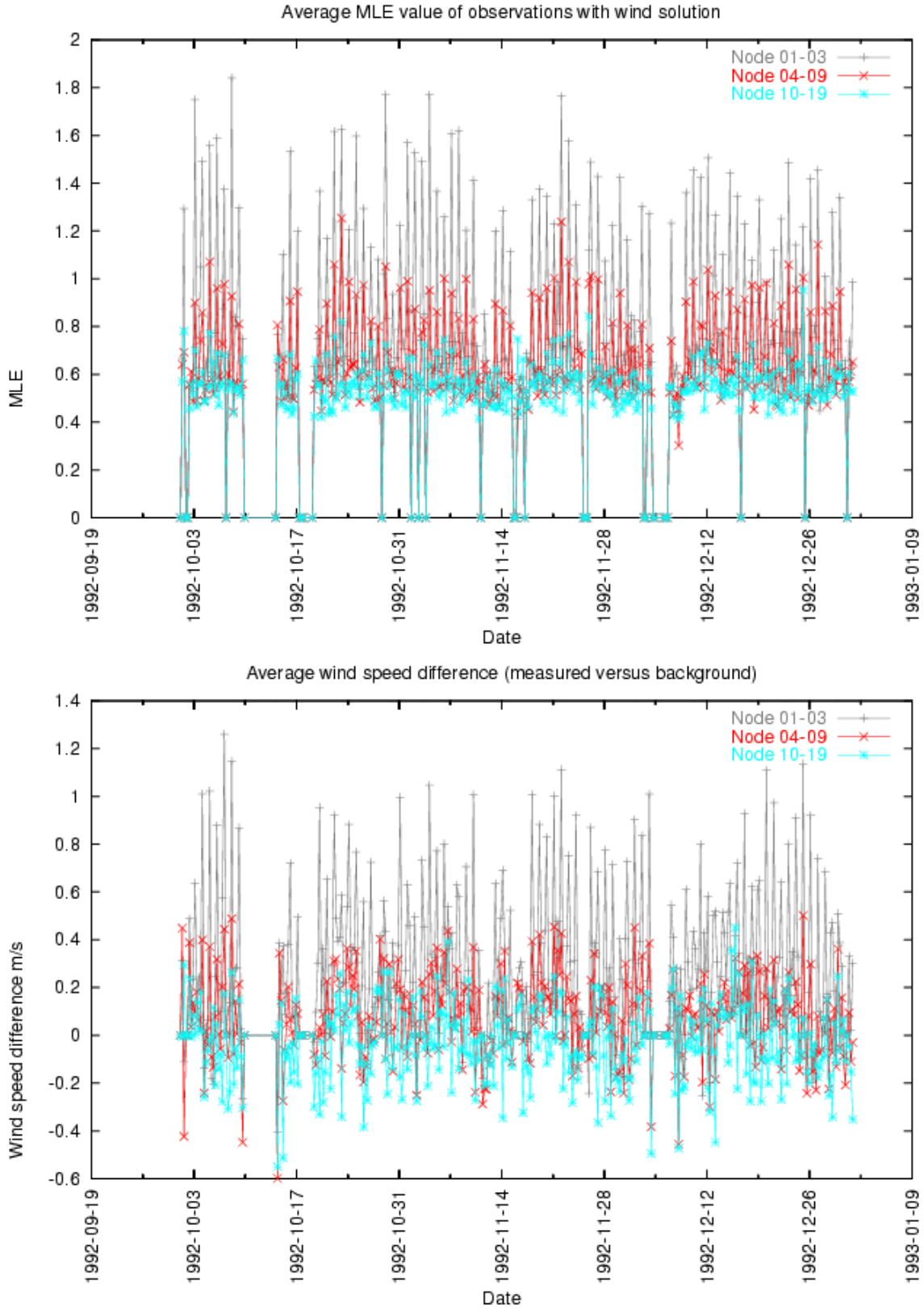

Figure 12a. Monitoring the ERS reprocessing for the 1st quarter of 1992. Each point represents a 6-hour average of inversion MLE (top) and wind speed bias with respect to ECMWF model (bottom).

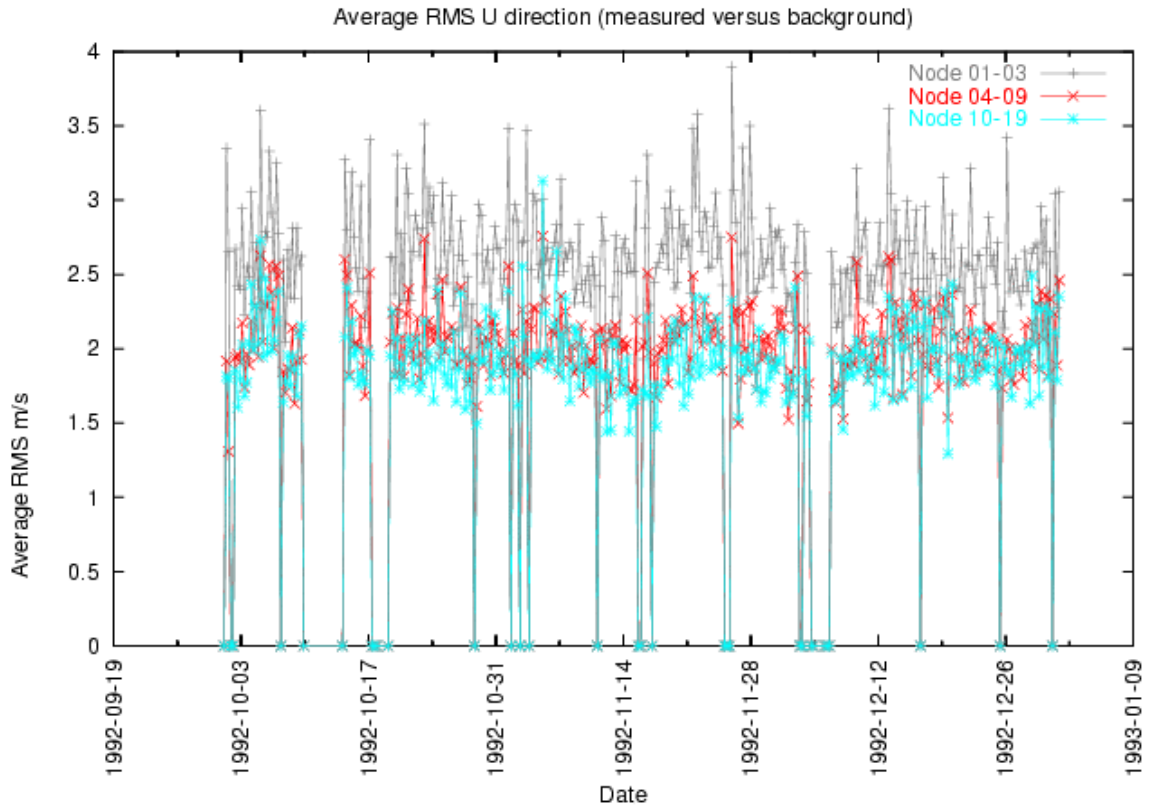

Figure 12b. Monitoring the ERS reprocessing for the 1st quarter of 1992. Each point represents a 6-hour average of the across-swath wind component RMS of ERS 1 minus ECMWF model.

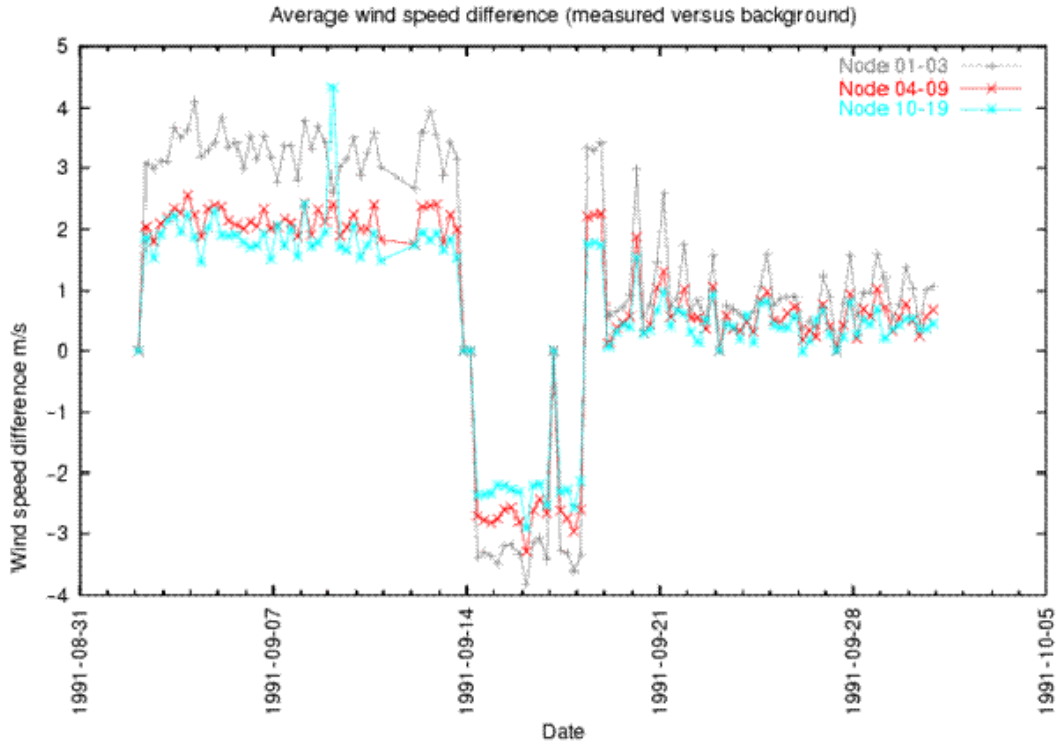

Figure 12c. As figure 12a bottom, but for September 1991.

Figure 12c is from the third quarter of 1991 where ERS 1 was still in its Cal/Val. It is clear that the instrument was not yet stable in that period.

ERS 1 data are available from Sep 2, 1991 until Jun 3, 1996, but there are some periods with data of questionable quality (see also Lecomte et al, 1999):

- Sep 2, 1991 to Mar 1, 1992 - Cal/Val, data were not put into MOS
- Mar 31, 1992 to Apr 13, 1992 - Large MLE and RMS values, data were not put into MOS
- Dec 23, 1993 to Jan 13, 1994 - Large MLE and RMS values, MARS data were replaced by reprocessed data available from Cersat, see below

ERS 2 data are available from Nov 22, 1995 until Jan 17, 2001, but there are also some periods with data of questionable quality (see also Lecomte et al, 1999):

- Nov 22, 1995 to Mar 19, 1996 - Cal/Val, data were not put into MOS
- Jan 16, 2001 to Jan 17, 2001 - degraded quality, data were not put into MOS

One period (Dec 23, 1993 to Jan 13, 1994) with questionable data quality was replaced by Cersat data, downloaded from http://www.ifremer.fr/cersat/en/data/download/swath/wnf.htm. The data were converted from Cersat format into BUFR. The BUFR files were sent to ECGATE and from there, step 1 and step 2 were followed.

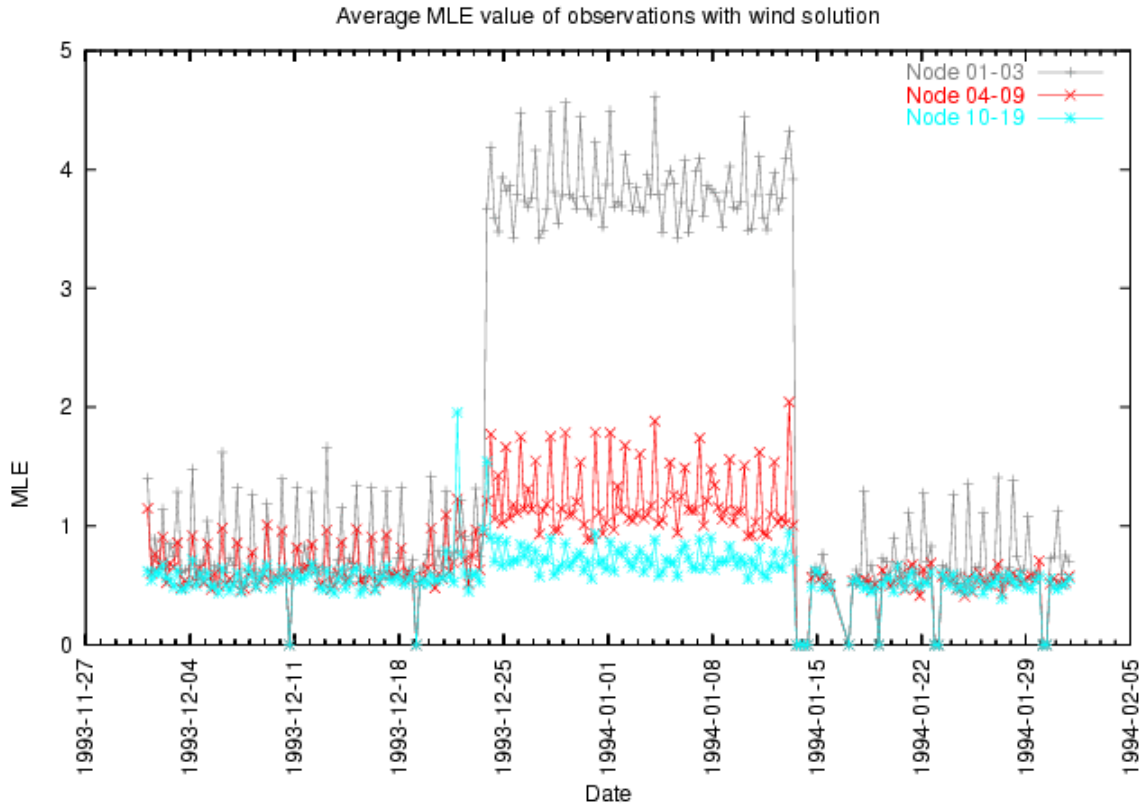

Figure 13a. As figure 12a top, but around Christmas 1993. Each point represents a 6-hour average of cone distance.

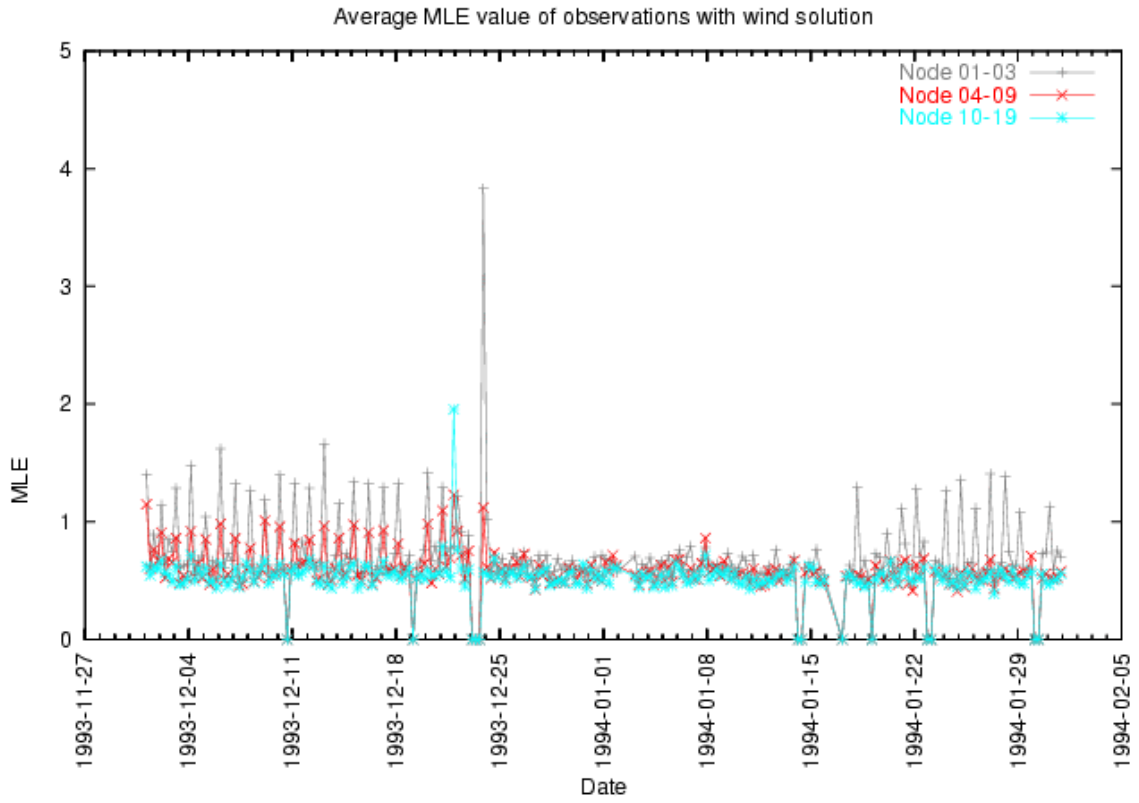

Figure 13b. As figure 13a, but after reprocessing with Cersat data.

Figure 13a shows the MLE values of end 1993 and beginning of 1994, with data taken from MARS. Figure 13b shows the same data, but now with the data of Dec 23 – Jan 13 replaced by data available from Cersat. This constitutes a short period that has been reprocessed by ESA and incorporated in the Cersat archive.

For the period Mar 31, 1992 to Apr 13, 1992, no data seem to be present at Cersat.

4.1.3 Step 3: calculation of wind stress from reprocessed ERS data

The data which have been reprocessed in step 2, were taken from the MOS, reprocessed and put back into the MOS in ASCII format. The stress processing was done on a Linux workstation. The stresses were calculated initially by simply multiplying the winds by a factor of 4.07×10^{-2}. In chapter 2 a modification is proposed.

5 Swath to grid conversion

5.1 Swath data coverage

There are observations from 2 March 1992 until 15 January 2001. In figure 14 the number of observations per 30 days is shown. This number increases gradually over the first two years as the operating schedule was being optimized. In 1996 the number almost doubles as both ERS-1 and ERS-2 contribute, followed by a few months in which ERS-2 did not function well. Overall, on the monthly time scale the observation density is reasonably constant, so that we do not expect large variations of the resulting fields in time.

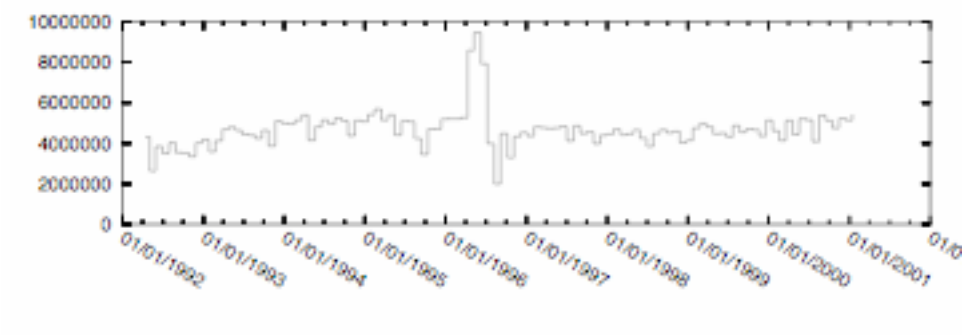

Figure 14. Number of observations per 30 days

The observation coverage is not very constant on the 6-hourly time scale (Figure 15), with several gaps indicating empty 6-hourly fields.

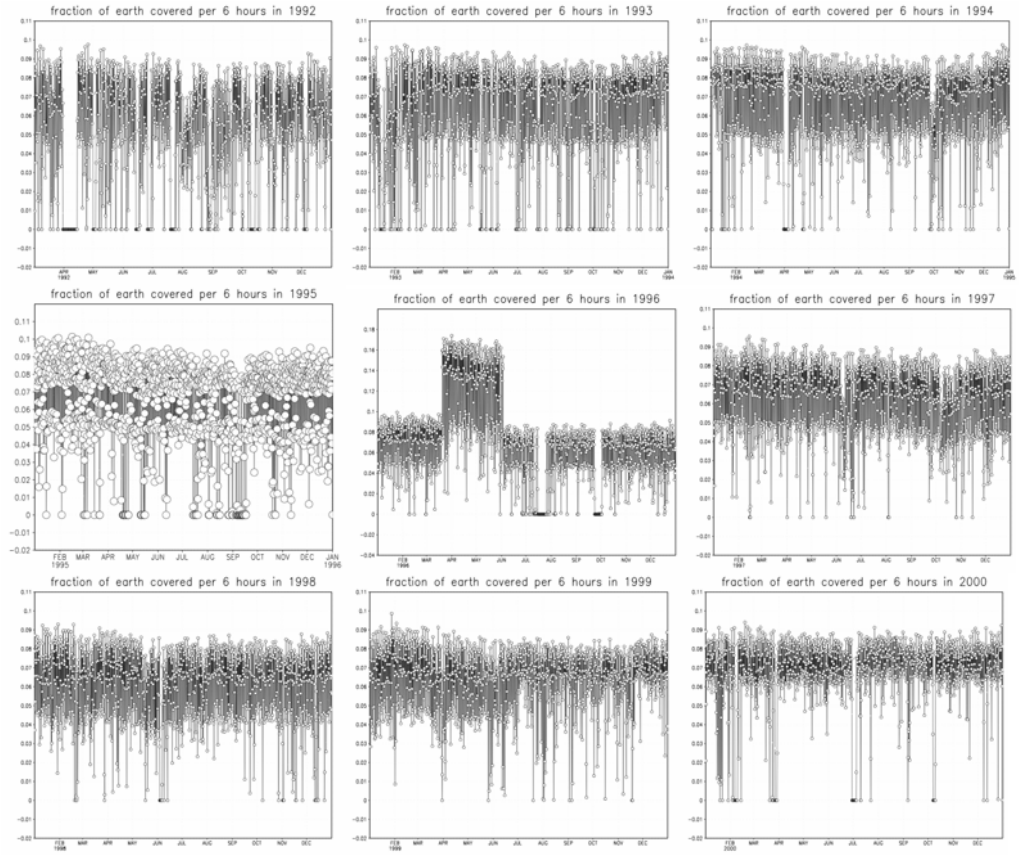

Figure 15. Fraction of earth covered by observations per 6 hours

In Figure 16 we show the number of observations per day and 0.5º by 0.5º grid box. A few features are obvious from this figure.

- Near continents with east-west coasts the coverage is poor, this is due to the time the instrument takes to switch from SAR mode (over land) to wind/wave mode (over sea)
- Between Antarctica and South America, Australia, and to a lesser extend South Africa, coverage is poor as these short ocean stretches are often used to switch off the scatterometer instrument (see also *Lecomte et al*, 1999).
- There are swaths of reduced coverage in the Indian and eastern Pacific Ocean, and on the northern Atlantic; these disappear in 2000 due to an improved data transmission mode.

Due to these differences the quality of the derived fields varies greatly with geographical location.

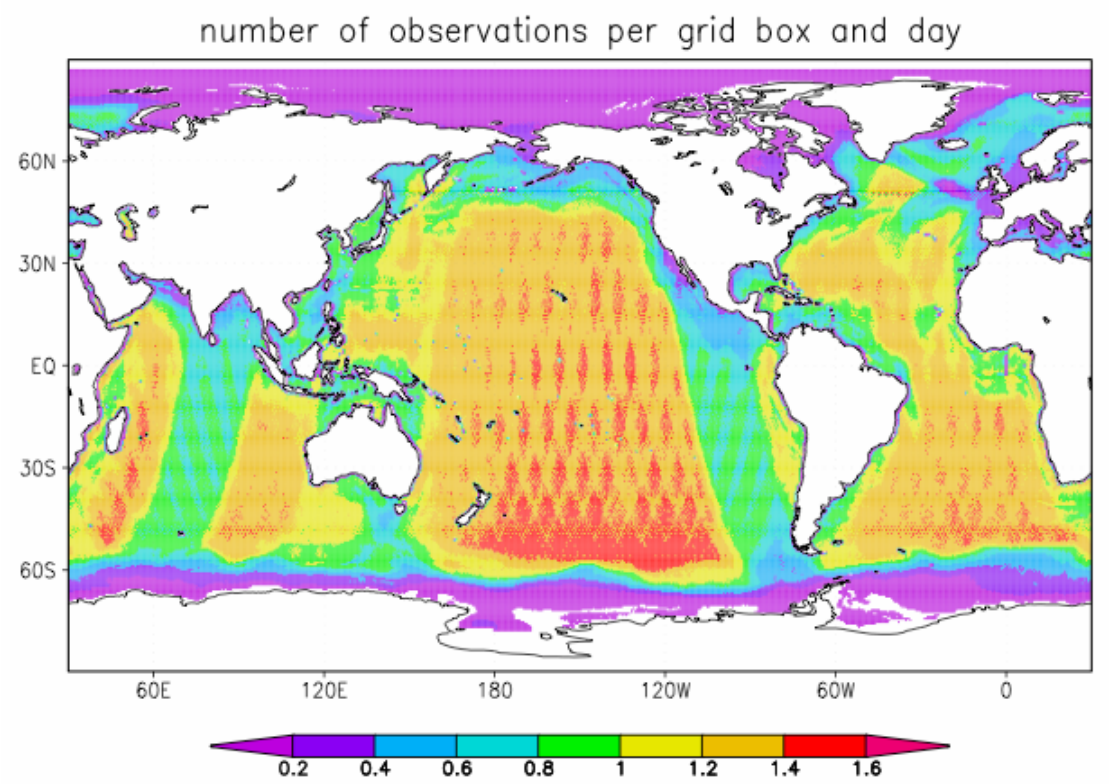

Figure 16. The number of along-track observation per day and per 0.5º grid box

The typical gaps between observations in space and time cannot easily be read off from Figure 16, as this also counts adjacent along-track data points that happen to fall in the same grid box. We therefore gathered all observations within 6-hour interval (comparable to the decorrelation scale of the wind) and computed how far apart these were on average. This repeat frequency is shown in Figure 17. It varies from less than once every 5 days off east-west coast, west of Ireland and in the Arctic Ocean, to about 3 days in most oceans, to 1.5 day in the Southern Ocean where the tracks are closer together.

Figure 17. The average number of days between observations in 6-hour intervals

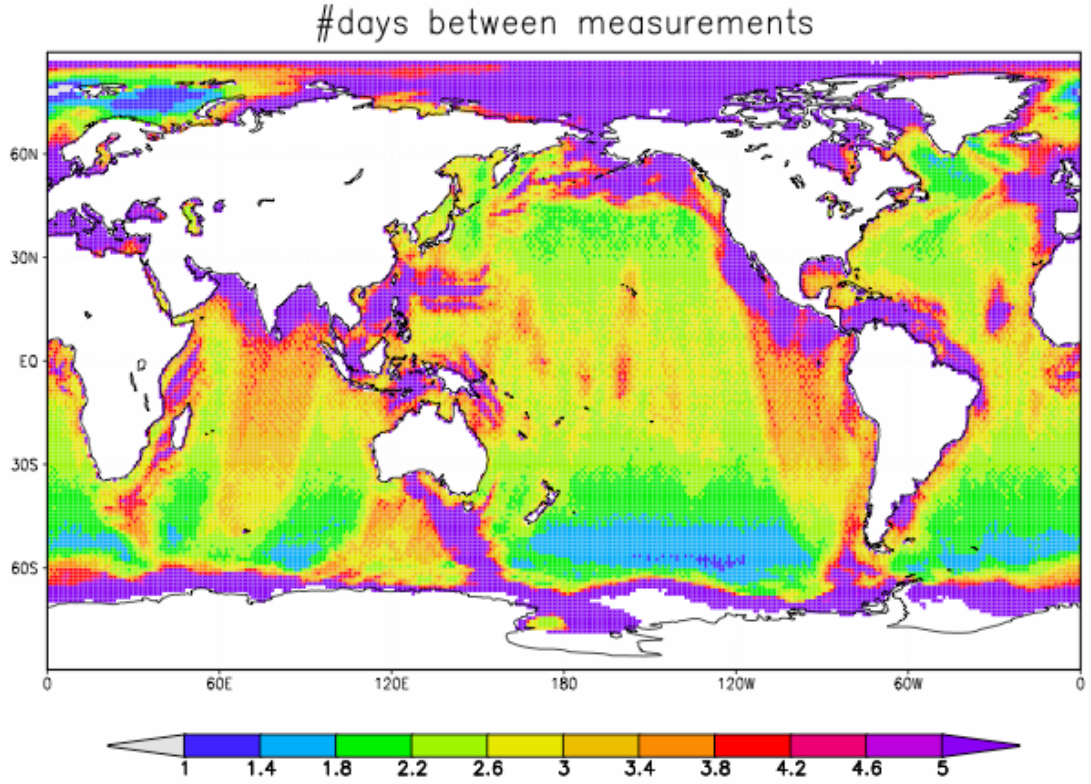

5.2 Decorrelation scales

To mesh with meteorological practice that is based on typical decorrelation scales in the atmosphere, we made 6-hourly lat-lon fields at 0.5º resolution. All along-track observations within a grid box and 6 hour interval are simply averaged, with duplicate observations rejected. Next, undefined grid points with 2 or more defined values in the surrounding 8 points are set to the average at these points, this fills in holes because of the mismatch between the along-track grid and the lat-lon grid, especially at high latitudes. This interpolation increases the number of grid boxes with valid data by about 20%.

As was already indicated in figure 15 and figure 17 the coverage of these 6-hourly fields is very incomplete at 10% of the earth (15% of the ocean) on average. As an example of the coverage in space and time we show in figure 18 the regions with data along the equator at a random time. One sees that the gaps are mostly larger than 10º and a few days.

The decorrelation lengths of the synoptic-scale variability has been determined by first applying a high-pass filter to the data (anomalies with respect to a 30-day running mean, this also eliminates the seasonal cycle), and next computing the correlation in space and time in 5º by 10º boxes. These correlations are fitted to a 3D Gaussian function. The correlations are shown in figure 19. On the equator one sees that in space, the autocorrelation drops off to less than 0.7 within 1.5º, in time it takes about 12 hours. In the storm track the scales are larger, about 2.5º SW-NE and 10º NW-SE, and 12 hours in-place in time, but much higher eastwards. This is of course due to the large-scale organization of depressions in this area.

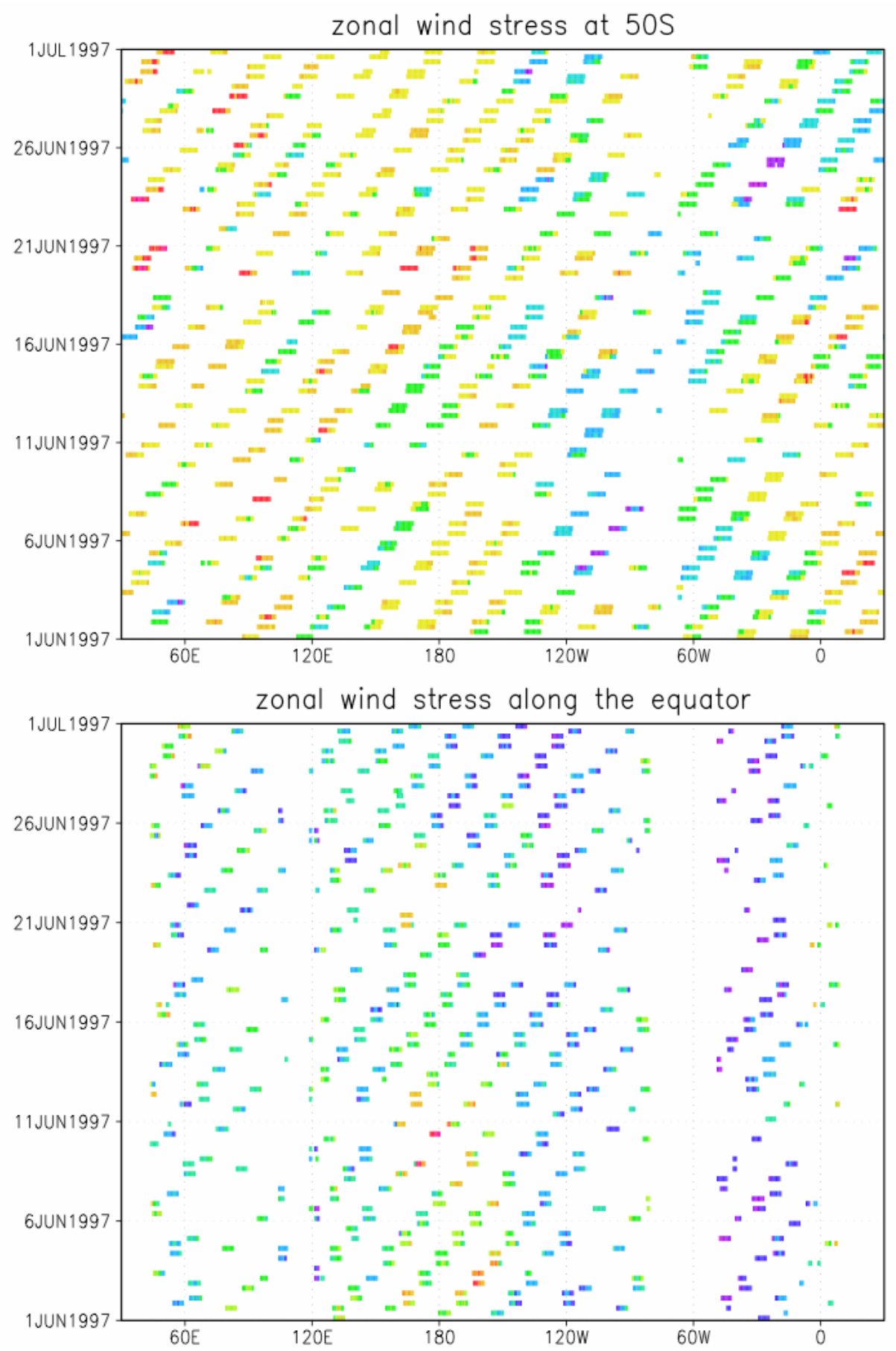

Figure 18. Observations of zonal wind along 50ºS, the equator and 50ºN in a random month

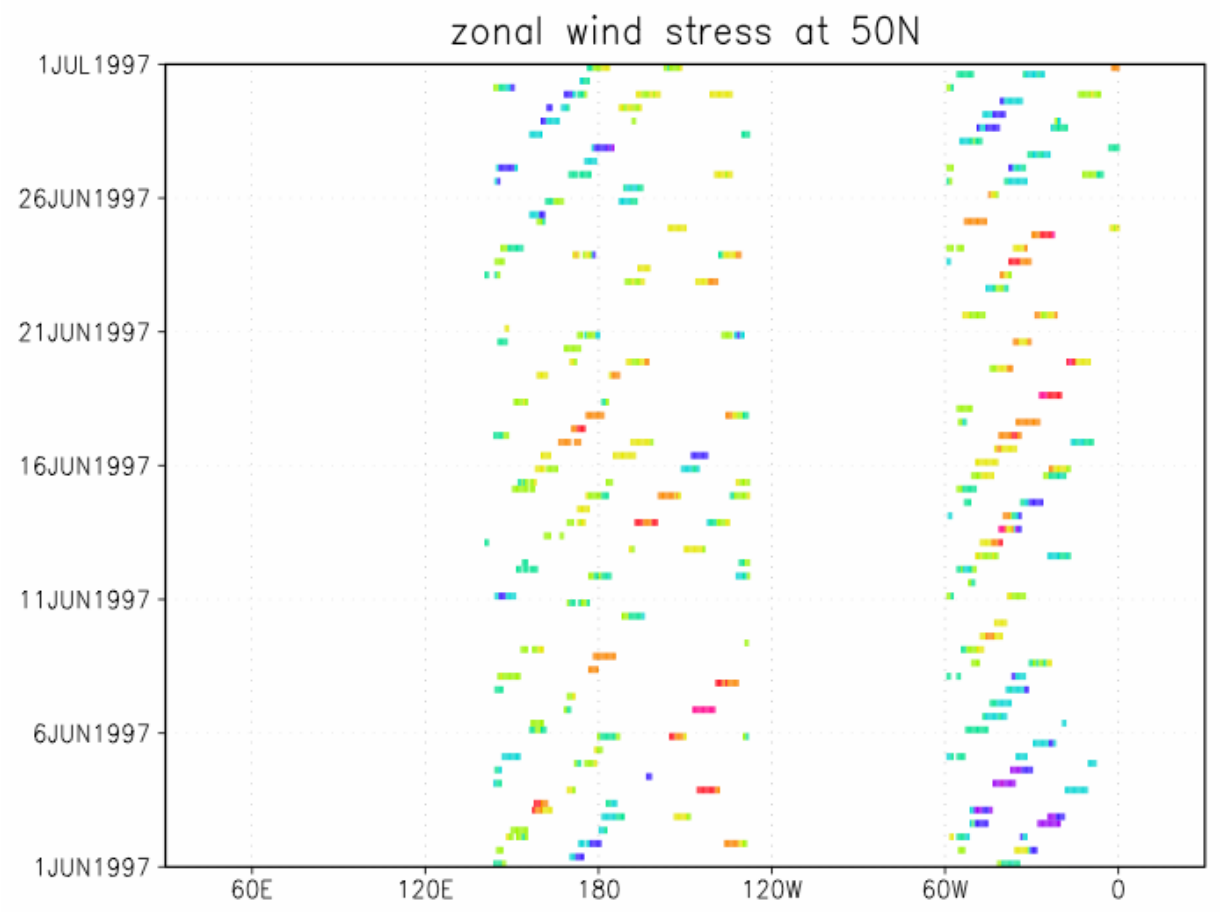

Figure 18. Continued

The fit parameters for the whole world are shown in figure 20. These are 7º-10º zonally, half this meridionally for zonal wind, smaller for meridional wind. In time the decorrelation scale is 12 hours or less.

One sees that interpolation between the ERS tracks is impossible as the distance between tracks is (much) larger than the decorrelation scales. We contemplated blending with calibrated ERA-40 data, but the resulting dataset would be dominantly re-analysis data with very little scatterometer input.

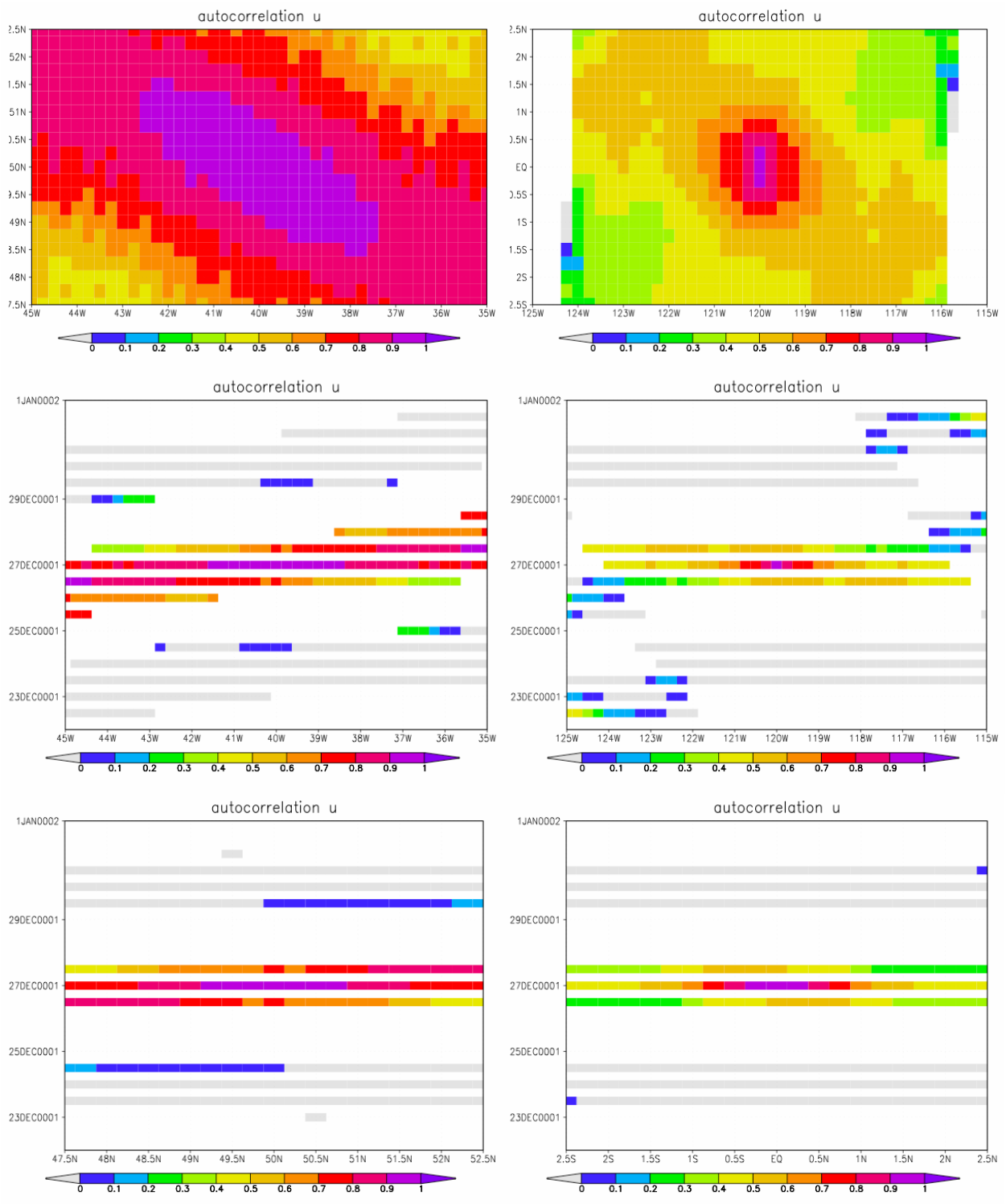

Figure 19. Autocorrelations of zonal wind in 47.5º-52.5ºN, 35º-45ºW (left) and 2.5ºS-2.5ºN, 115º-125ºW (right)

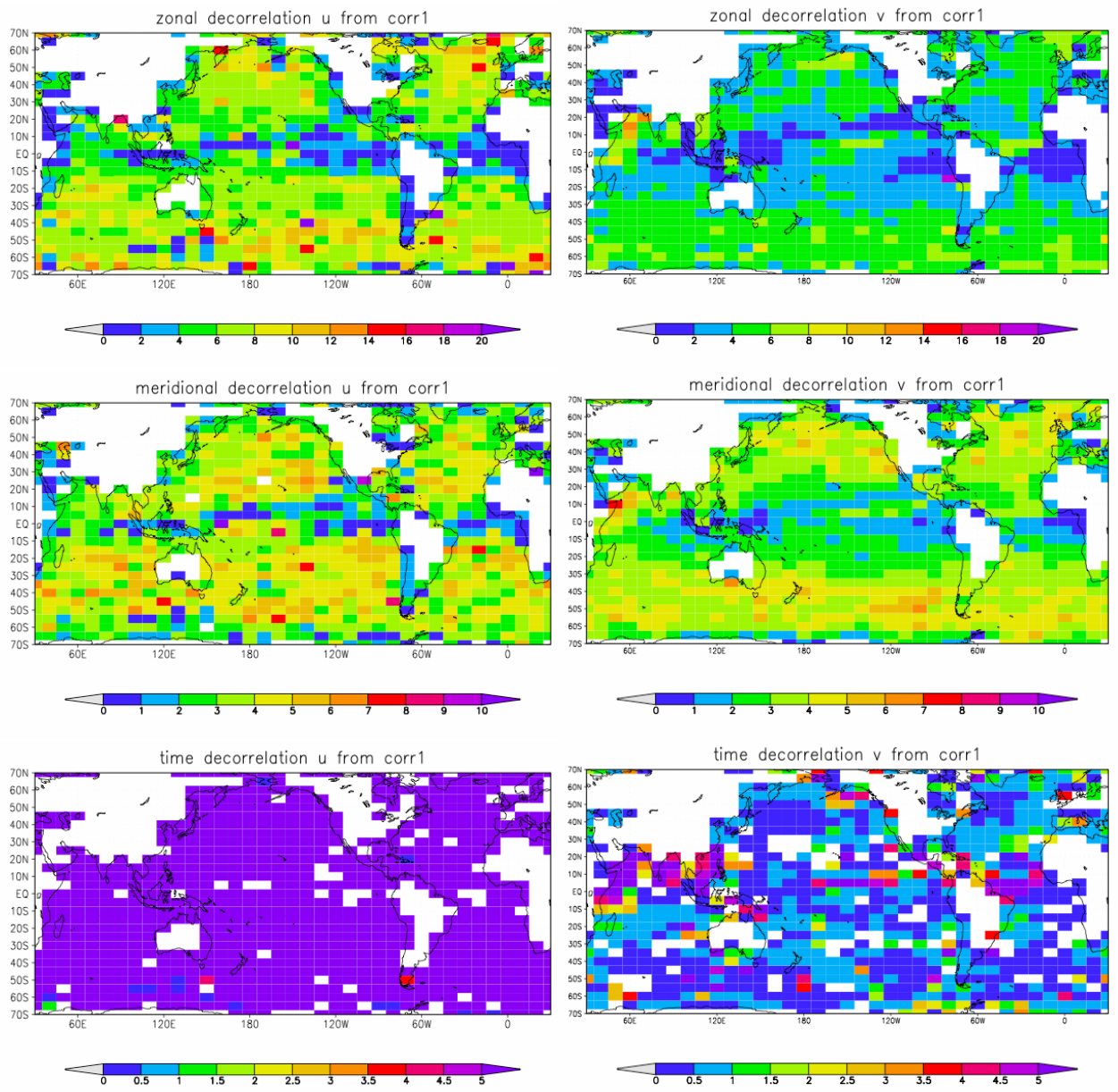

Figure 20. The zonal, meridional and time decorrelation lengths (in degrees and days) of the high-frequency features in the zonal and meridional wind (1999 data only).

5.3 6-hourly fields

We have made available on the KNMI Climate Explorer (van *Oldenborgh en Burgers* 2005, climexp.knmi.nl) 6-hourly fields without interpolation between the tracks. These are in the form of yearly fields at 0.5º resolution, which are just under 2GB uncompressed. They can be downloaded as grads files, netcdf, and hdf5.

These should be compared to the fields of *Milliff* et al (2004), available as ds744.4 at UCAR. These are QuikScat fields for 1999-2004, where the gaps have been filled using the NCEP

reanalysis (*Kalnay* et al, 1996). The SeaWinds scatterometer has a much larger coverage, 90% of the ocean every 24 hours.

To compare our fields with these we used the time window as in *Milliff* et al: the 0-6 UTC and 6-12 UTC fields were averaged to obtain the 6 UTC value, for 12 UTC the 6-12 and 12-18 UTC fields were averaged, etc. The spatial grid was also shifted by half a grid box for this comparison. The comparison was performed for 2000, the only year in which both products were available.

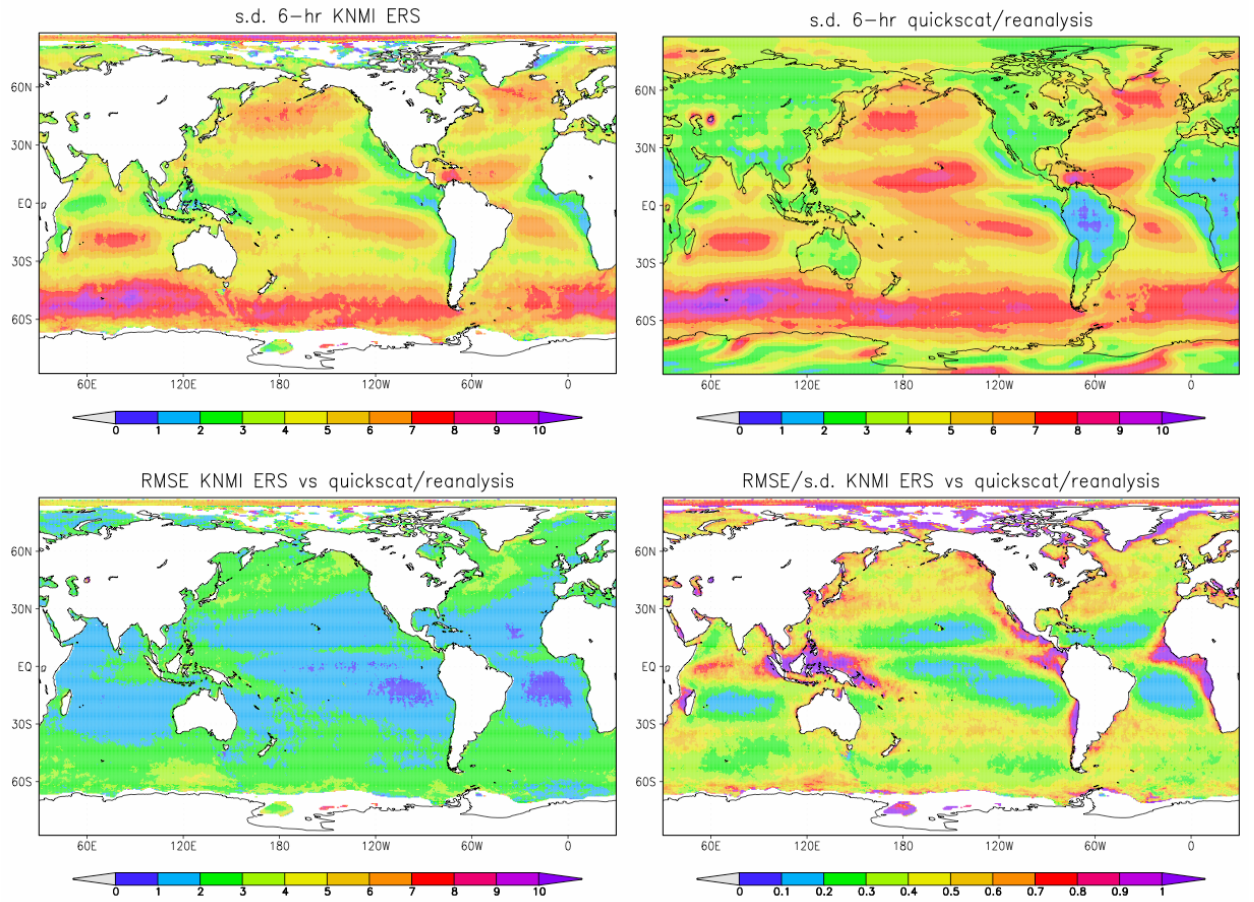

Figure 21. A comparison of the 6-hourly fields of our ERS re-analysis and the merged quickscat/reanalysis fields of *Milliff* et al.: standard deviation, RMSE and RMSE normalized to the standard deviation.

In figure 21 one sees that the standard deviation of the merged QuikScat/reanalysis fields is in general larger than our ERS analyses. After the merging high spatial frequency noise has been added to the areas without scatterometer data to keep the power spectrum the same. This noise may explain the higher standard deviation.

The RMS error between the fields varies from slightly less than 1 m/s in the calm subtropical oceans to more than 4 m/s in the storm tracks. The global average is close to 2 m/s. As a percentage of the standard deviation, the errors are large near coasts and in the Maritime Continent, and in the Arctic and Antarctic sea ice margins. Near coasts data coverage of our

analysis is poor. Over the Maritime Continent the reanalysis winds may suffer from poorly resolved islands. Near sea ice the observations may often correspond to high-wind situations when there is less ice, leading to a biased estimate. The ERS product appear suspicious close to the North Pole where no winds are expected. Alternatively, the SeaWinds product is known to have problems there; this would need to be improved in a SeaWinds reprocessing.

The remaining differences are quite large, 20-50% of the standard deviation over most of the oceans. These are due to the addition of noise to the reanalysis data when there is no QuikScat data, and the long time window of 12 hours, which means that on average one compares observations that are more than 4 hours apart (in RMS), which is already a sizeable fraction of the decorrelation scale.

5.4 Monthly fields

Due to the decorrelation scale being smaller than the gaps between observations in general, the half dozen or so observations every month can be considered a sample of the true average wind (stress) during that month. A straight average of these points therefore gives a sensible monthly mean field. These have also been made available in the Climate Explorer. At this web site one can easily compare this product with other estimates of wind and wind stress. All figures in the following have been generated directly in the web site.

In figure 22 we show the standard deviation of the monthly zonal wind anomalies in the KNMI ERA analysis described here, the Ifremer ERS analysis (*Quilfen* et al, 2001, www.ifremer.fr/cersat/en/data/download/download.htm) and the ERA40 (*Uppala* et al, 2005) and NCEP/NCAR reanalyses. One sees that the Ifremer analysis, which does interpolate between tracks, therefore missing high-frequency variability and underestimates the standard deviation, especially in the eastern tropical Pacific, Atlantic and Indian Oceans (where the track patterns is clearly visible in the Ifremer product). These regions have very short decorrelation scales (figure 20). Also in areas with coverage problems, such as south of Australia, the Ifremer product underestimates variability. On the other hand the KNMI product is noisier. Both reanalyses severely underestimate variability in the eastern part of the tropical oceans. The NCEP/NCAR product also shows a model bias in the central Pacific, where zonal wind is an important part of the ENSO cycle.

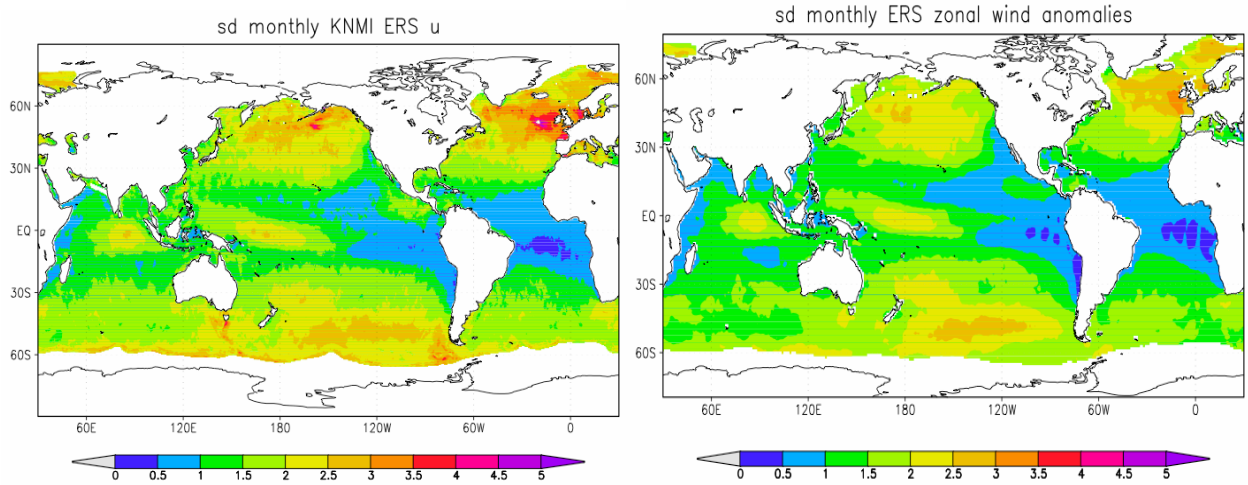

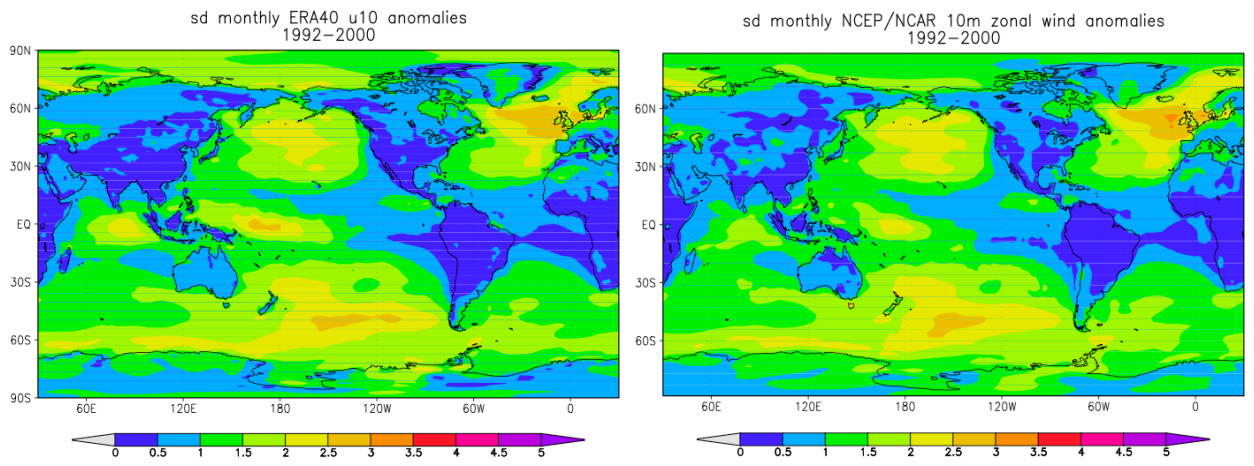

Figure 22. The standard deviation of zonal wind anomalies [m/s] in the KNMI, Ifremer ERS analyses and the ERA40, NCEP/NCAR reanalyses.

These differences also show up in the RMSE and regression maps of figure 23. The RMS error is large south of Australia and South-America and near east-west coasts, where the scatterometer was often turned off (figure 16). Ifremer analysis is seen to have regression coefficients <1 in the tropical ocean between tracks where the decorrelation lengths are small. However, the difference with the reanalysis wind fields is much larger, especially with the NCEP/NCAR winds, probably due to model error entering the reanalyses and their inability to capture the small-scale variability in these regions.

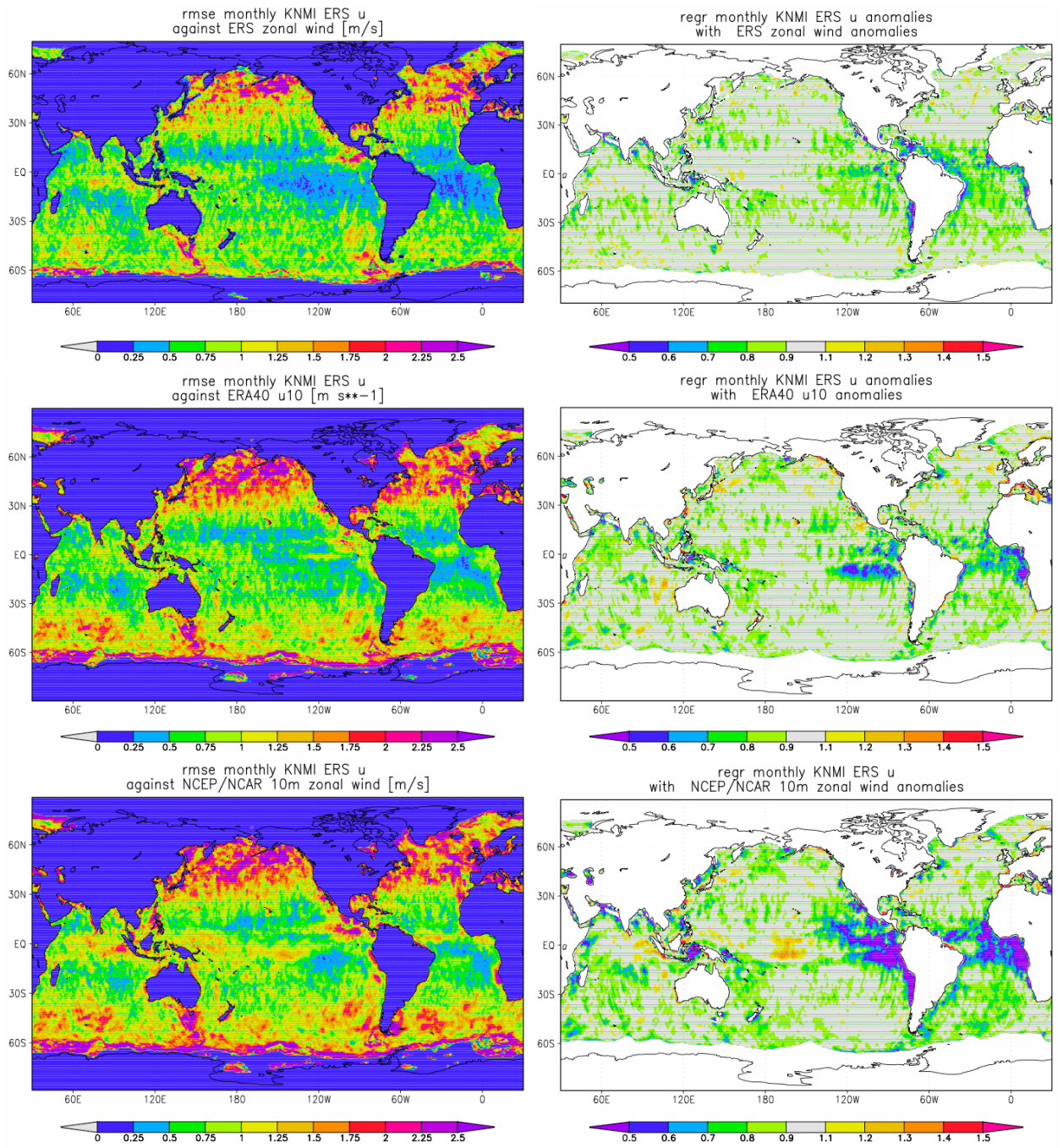

Figure 23. RMSE difference and regression of other wind products on the KNMI ERS analyses

6 Concluding

A Scatterometer Ocean Stress (SOS) product has been developed in the context of the Climate Monitoring SAF as described in this report. First, ten years of ERS scatterometer data are reprocessed with the most up-to-date wind processor (ESDP), including improvements in QC, C-band geophysical model (CMOD5), its inversion, ambiguity removal, and quality monitoring.

A detailed and accurate wind-to-stress study using triple collocated observations of buoys, ERS scatterometer and NWP winds in combination with the ECMWF and the LKB surface layer models is reported on, leading to a recommendation for global wind to stress conversion.

The spatial and temporal characteristics of the ERS scatterometer sampling and winds are carefully analyzed in order to develop gridded SOS products.

The user need for such product is motivated from the fact that NWP (re)analysis fields do not encapsulate the mesoscale detail as observed by scatterometers. Since NWP meteorological analyses necessarily constitute so-called low pass filter characteristics, such mesoscale detail remains absent after the assimilation of scatterometer winds. Moreover, observed detail in the wind field at the ocean inertial scales corresponding to these scatterometer-observed phenomena is important for the forcing of ocean circulation models that are used in routine operations and for climate studies. Several oceanographic and climate community users therefore request SOS products.

As such, we recommend a commitment to routine / operational SOS responsibilities for ASCAT, including reprocessing facilities for gridded products. SeaWinds scatterometer data would further bridge the ERS data base into the ASCAT era. The SeaWinds data coverage is representative of ASCAT, whereas the ERS coverage is more limited.

On the longer term, ASCAT improved SOS gridded products could be envisaged. Moreover, resources permitting, the abundant winds from passive microwave sounders may be investigated for use in the gridded wind stress products as these present improved temporal coverage, though lack good information on wind direction. For example, such products may resolve the diurnal cycle as present in semi-enclosed seas such as the Mediterenean.

7 Appendix

In order to make sure that the LKB software version that we use is consistent with the original one presented by Liu and Tang (1996), we successfully reproduce Figure 1 of their report, which shows the ratio of equivalent neutral wind to actual wind at 10 m for various air-sea temperature differences and wind speeds, assuming a constant rh of 0.7 and a SST of 15°C. Figure A.1 shows a similar plot, although using a set of parameters more representative of tropical TAO observations, i.e., z = 4 m, rh = 0.8, and SST = 26.5°C. We note that for a certain unstable stratification (constant rh and air-sea temperature difference), the ratio between neutral and actual wind is decreasing with increasing wind speeds. Given that the mean air-sea temperature difference in the tropics for TAO/PIRATA buoys is around -0.8°C (see Figure A.2), the mentioned ratio is already below 10% at 5 m/s winds and decreases with speed (see Figure A.1).

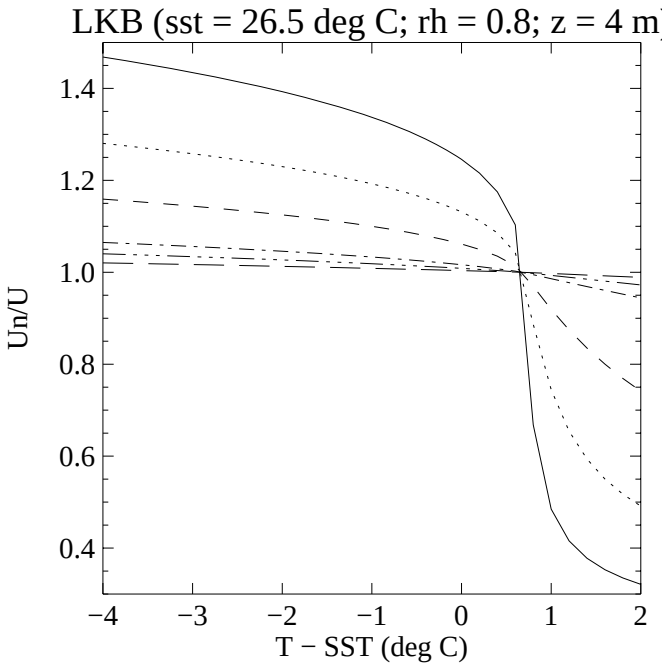

Figure A.1. Ratio of equivalent neutral wind to actual wind at 4 m height as a function of air-sea temperature differences, assuming a constant rh of 0.8 and a SST of 26.5°C, for various wind speeds: 0.5 m/s (solid), 1 m/s (dotted), 2 m/s (dashed), 5 m/s (dash dot), 7 m/s (dash-dot-dot-dot), and 10 m/s (long dashes).

In order to maintain a constant 10% difference between neutral and actual wind (ratio of 1.1 in Figure A.1), not only strong instability is needed but also a very strong air-sea temperature dependence on wind speed, i.e., instability (negative air-sea temp. difference) should substantially increase for increasing speeds. Figure A.2 shows the air-sea temperature histogram for our TAO/PIRATA dataset[1], for all speeds (solid) and several speed ranges. As it is discernible, strong

[1] Please, note that Liu and Tang used more than 8 years (July 1986 to March 1995) of TAO buoys 0n165e and 0n110W to produce their results, while we use 1 year (2000) of all available TAO/PIRATA buoys as described in section 3.2.

instability (air-sea temp. difference below -3°C) is seldom and there is no stability dependency on wind speed whatsoever (all the distributions in Figure A.2 have similar mean values).

Therefore, from these results, one can not explain a 10% difference between neutral and actual winds for TAO observations. Moreover, Figures A.1 and A.2 are consistent with the results shown in Figure 8.

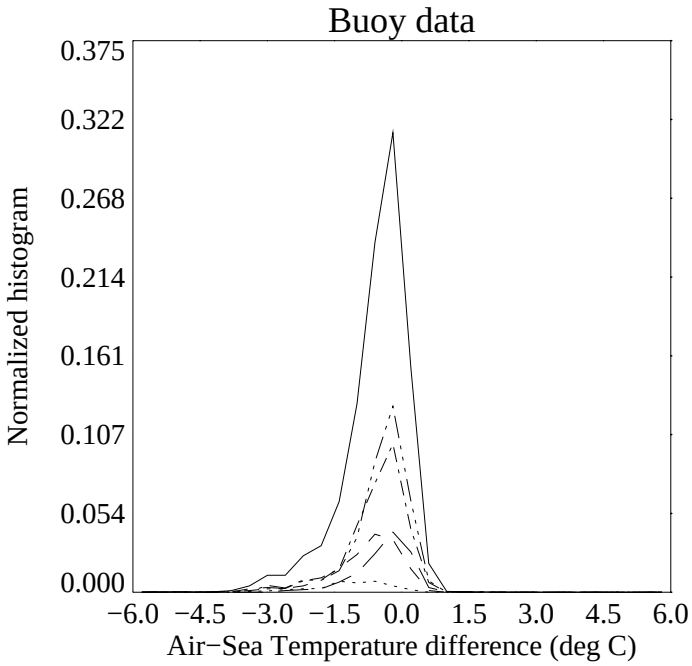

Figure A.2. Histogram of TAO/PIRATA air-sea temperature difference, for all speeds (solid) and several speed ranges: below 2 m/s (dotted), 2-4 m/s (dashed), 4-6 m/s (dash dot), 6-8 m/s (dash-dot-dot-dot), and 8-10 m/s (long dashes).

8 References

Attema, E. P. W., "The active microwave instrument on board the ERS-1 satellite," *Proc. IEEE*, vol. 79, pp. 791-799, 1991.

Beljaars, A.C.M., "Air-sea interaction in the ECMWF model," *Proc. of seminar on atmosphere-surface interaction*, European Centre for Medium-Range Weather Forecasts, Reading, United Kingdom, 1997.

Bourassa, M.A., "Satellite-based observations of surface turbulent stress during severe weather," (Chapter 2), *Atmosphere-Ocean Interactions*, vol. 2, ed., W. Perrie, Wessex Institute of Technology, pp. 35-52, 2006.

Businger, J.A., "Turbulent transfer in the atmospheric surface layer," *Workshop on Micrometeorology*, Amer. Meteorol. Soc., pp. 67-100 1973

Businger, J.A., "Interactions of sea and atmosphere," *Rev. Geophys. Space Phys*., vol. 13, pp. 720-822, 1975.

Charnock, H., "Wind stress on a water surface," Q. J. R. Meteorol. Soc., vol. 81, pp. 639-640, 1955.

Chelton D.B., and Schlax, M.G., "Global observations of oceanic Rossby waves," *Science*, vol. 272, pp. 234-238, 1996.

Chelton, D.B., Esbensen, S.K., Schlax, M.G., Thum, N., Freilich, M.H., Wentz, F.J., Gentemann, C.L., McPhaden, M.J., and Schopf, P.S., "Observations of coupling between surface wind stress and sea surface temperature in the eastern Tropical Pacific," *J. Climate*, vol. 14, pp. 1479-1498, 2001.

Chelton, D.B., Schlax, M.G., Freilich, M.H., Millif, R.F., "Satellite measurements reveal persistent small-scale features in ocean winds," *Science*, vol. 303, pp. 978-983, 2004.

Donelan, M.A., Dobson, F.W., Smith, S.D., and Anderson, R.J., "On the dependence of sea surface roughness on wave development," *J. Phys. Oceanogr.*, vol. 23, pp. 2143-2149, 1993.

Friehe, C.A., and Schmitt, K.F., "Parameterization of air-sea interface fluxes of sensible heat and moisture by bulk aerodynamic formulas," *J. Phys. Oceanogr.*, vol. 6, pp. 801-809, 1976.

Garrat, J.R., "Review of drag coefficients over oceans and continents," *Mon. Wea. Rev.*, vol. 105, pp. 915-929, 1977.

Geernaert, G.L., "Theory of air-sea momentum, heat and gas fluxes," in *Air-sea exchange: physics, chemistry, and dynamics*, ed. G.L. Geernaert, Kluwer Academy Publishers, Boston, pp. 25-48, 1999.

Hersbach, H., A. Stoffelen, and de Haan, S., "The improved C-band ocean geophysical model function CMOD-5", *J. Geophys. Res.*, vol. 112 (C3), doi:10.1029/2006JC003743, 2007.

Kalnay, E., M. Kanamitsu, R. Kistler, W. Collins, D. Deaven, L. Gandin, M. Iredell, S. Saha, G. White, J. Woollen, Y. Zhu, M. Chelliah, W. Ebisuzaki, W. Higgins, J. Janowiak, K. C. Mo, C. Ropelewski, J. Wang, A. Leetmaa, R. Reynolds, R. Jenne, and D. Joseph, 1996: The NMC/NCAR 40-Year Reanalysis Project". Bull. Amer. Meteor. Soc., 77, 437-471.

Kelly, K.A., Dickinson, S., McPhaden, M.J., and Johnson, G.C., "Ocean currents evident in satellite wind data," *Geophys. Res. Lett.*, vol. 28(12), pp. 2469-2472, 2001.

KNMI Climate Explorer, http://climexp.knmi.nl

KNMI scatterometer site, http://www.knmi.nl/scatterometer

Lecomte et al., Three contributions in Proc. "Emerging Scatterometer Applications; From research to operations" ESTEC, Noordwijk, The Netherlands, 5-7 October 1998, ESA SP-424, 1999.

Liu, W.T., Katsaros, K.B., and Businger, J.A., "Bulk parameterization of air-sea exchanges of heat and water vapor including the molecular constraints in the interface," *J. Atmos. Sci.*, vol. 36, 1979.

Liu, W.T., and Tang, W., "Equivalent neutral wind," *Jet Propulsion Laboratory 96-17*, Pasadena, USA, August 1996.

Milliff, R.F., "Forcing global and regional ocean numerical models with ocean surface vector winds from spaceborne observing systems," in *Proc. 2nd Ocean and Sea Ice SAF Workshop*, EUM P.45, ISBN 1561-1485, Perros-Guirec, France, 15-17 March, 2005.

Milliff, Ralph F., Morzel, Jan, Chelton, Dudley B., Freilich, Michael H. 2004: Wind Stress Curl and Wind Stress Divergence Biases from Rain Effects on QSCAT Surface Wind Retrievals. Journal of Atmospheric and Oceanic Technology: Vol. 21, No. 8, pp. 1216--1231.

Milliff, R.F., and Morzel, J., "The global distribution of the time-average wind stress curl from NSCAT," *J. Atmos. Sci.*, vol. 58 (2), 2001.

Monin, A.S., and Obukov, A.M., "Basic regularity in turbulent mixing in the surface layer of the atmosphere," *USSR Acad. Sci. Geophys. Inst.*, No 24, 1954.

Offiler, 1994, J. Atm. Ocean Techn.

Oldenborgh, G.J. van and G. Burgers, *Searching for decadal variations in ENSO precipitation teleconnections*, Geophys. Res. Lett., 2005, 32, 15, L15701, doi:10.1029/2005GL023110

OSI SAF, http://www.eumetsat.de/en/area4/saf/internet/main_safs/osi/main_osisaf.html

Quilfen, Y., Chapron, B., Vandemark, D., 2001, "The ERS Scatterometer Wind Measurement Accuracy: Evidence of Seasonal and Regional Biases", J. Atmospheric and Oceanic Technology, vol. 18, no. 10, pp. 1684-1697.

Park, K.A., Cornillon, P., and Codiga, D., "Modification of surface winds near ocean fronts: effects of Gulf Stream rings on scatterometer (QuikSCAT, NSCAT) wind observations," *J. Geophys. Res.*, vol. 111,C 403021, doi:10.1029/2005JC003016, 2006.

Pond, S., Fissel, D.B., and Paulson, C.A., "A note on bulk aerodynamic coefficients for sensible heat and moisture fluxes," *Boundary Layer Meteorol.*, vol. 6, pp. 333-340, 1974.

Portabella, M., and Stoffelen, A., "Development of a global scatterometer validation and monitoring," *Visiting Scientist report for the EUMETSAT OSI SAF*, 2007.

Smith, S.D., Anderson, R.J., Oost, W.A., Kraan, C., Maat, N., DeCosmo, J., Katsaros, K.B., Davidson, K.L., Bumke, K., Hasse, L., and Chadwick, H.M., "Sea surface wind stress and drag coefficients: the HEXOS results," *Boundary Layer Meteorol.*, vol. 60, pp. 109-142, 1992.

Stoffelen, A., "Scatterometer Ocean Stress," *proposal to the CM-SAF*, Koninklijk Nederlands Meteorologisch Instituut, The Netherlands, available at http://www.knmi.nl/scatterometer/, 2002.

Stoffelen, A., "Error modeling of scatterometer, in-situ, and ECMWF model winds; a calibration refinement," *Technical report TR-193*, Koninklijk Nederlands Meteorologisch Instituut, The Netherlands, 1996.

Stoffelen, A., "Scatterometry," *PhD thesis at the University of Utrecht*, ISBN 90-393-1708-9, October 1998a.

Stoffelen, A., 'Error modeling and calibration: towards the true surface wind speed," *J. Geophys. Res.*, vol. 103, no. C4, pp. 7755-7766, 1998b.

Taylor, P.K., and Yelland, M.J., "The dependence of sea surface roughness on the height and steepness of the waves," *J. Phys. Oceanogr.*, vol. 31, pp. 572-590, 2001.

Taylor, P.K., Yelland, M.J., and Kent, E.C., "On the accuracy of ocean winds and wind stress," *WCRP/SCOR Workshop on Intercomparison and Validation of Ocean-Atmosphere Flux Fields*, Bolger Center, Potomac, MD, USA, May 2001.

Uppala, S.M., et al, *The ERA-40 Reanalysis*, Quart. J. Royal Meteorol. Soc., **131**, 612, 2961-3012, doi:10.1256/qj.04.176., 2005.

Vialard, Jérôme, Seasonal forecasts and its requirements for satellite products, Proc. OSI SAF training workshop, pp. 137-143, ISBN 92-9110-034-X, EUMETSAT P27, Darmstadt, Germany, 2000.

Vogelzang, Jur, On the quality of high resolution wind fields, NWPSAF-KN-TR-002, v1.2, 2006, http://www.metoffice.gov.uk/research/interproj/nwpsaf/scatterometer/index.html .

9 Acknowledgements

We acknowledge the help and collaboration of our colleagues working at KNMI, and more in particular the people from the scatterometer group. This work is funded by the EUMETSAT Climate Monitoring (CM) SAF, lead by the DWD. ESA is greatly acknoweledged for providing the ERS scatterometer data and ECMWF and CerSat for storing the data. Moreover, NASA and NOAA are acknowledged for providing SeaWinds scatterometer data through the dataset of Milliff et al. The software used in this work has been developed at KNMI through the EUMETSAT Ocean and Sea Ice (OSI) and Numerical Weather Prediction (NWP) SAFs.

10 Glossary

ADEOS	(Japanese) Advanced Earth Observation Satellite
AR	Ambiguity Removal
ASCAT	Advanced Scatterometer
AWDP	ASCAT Wind Data Processor
BUFR	Binary Universal Format Representation
CERSAT	Centre ERS d'Archivage et de Traitement
CM SAF	Climate Monitoring SAF
DWD	German Weather Office (Deutche Wetterdienst)
ECMWF	European Centre for Medium-range Weather Forecasts
EPS	Eumetsat Polar System
ERA	ECMWF ReAnalysis
ERS	European Remote-Sensing Satellite
ESA	European Space Agency
ESDP	ERS Scatterometer Data Processor
ENSO	El Niño Southern Oscillation
EUMETCast	EUMETSAT’s Digital Video Broadcast Data Distribution System
EUMETSAT	European Meteorological Satellite Agency
FSU	Florida State University
GOES	Geostationary Operational Environmental Satellite
HDF	Hierarchical Data Format
HH	Horizontal polarisation send and receive mode
IR	InfraRed
JPL	Jet Propulsion Laboratory (NASA)
KNMI	Royal Netherlands Meteorological Institute
LKB	Liu Katsaros Businger

NASA	National (US) Air and Space Agency
NOAA	National (US) Oceanic and Atmospheric Administration
NSCAT	NASA Scatterometer
NWP	Numerical Weather Prediction
OSI SAF	Ocean and Sea Ice SAF
PBL	Planetary Boundary Layer
PIRATA	Pilot Research Moored Array in the Tropical Atlantic
QC	Quality Control
QuikScat	US dedicated scatterometer mission to bridge ADEOS-I and ADEOS-II
rh	relative humidity
RMDCN	Regional Meteorological Data Communication Network
SAF	Satellite Application Facility
SAR	Synthetic Aperture Radar
SeaWinds	US scatterometer on-board QuikSCat and ADEOS-II platforms
SL	Surface Layer
SOS	Scatterometer Ocean Stress
SST	Sea Surface Temperature
TAO	Tropical Array of Buoys
TRITON	Triangle Trans Ocean buoy Network
VV	Vertical polarisation send and receive mode
WVC	Wind Vector Cell